iScience

Article

A subunit vaccine Ag85A-LpqH focusing on humoral immunity provides substantial protection against tuberculosis in mice

Graphical abstract

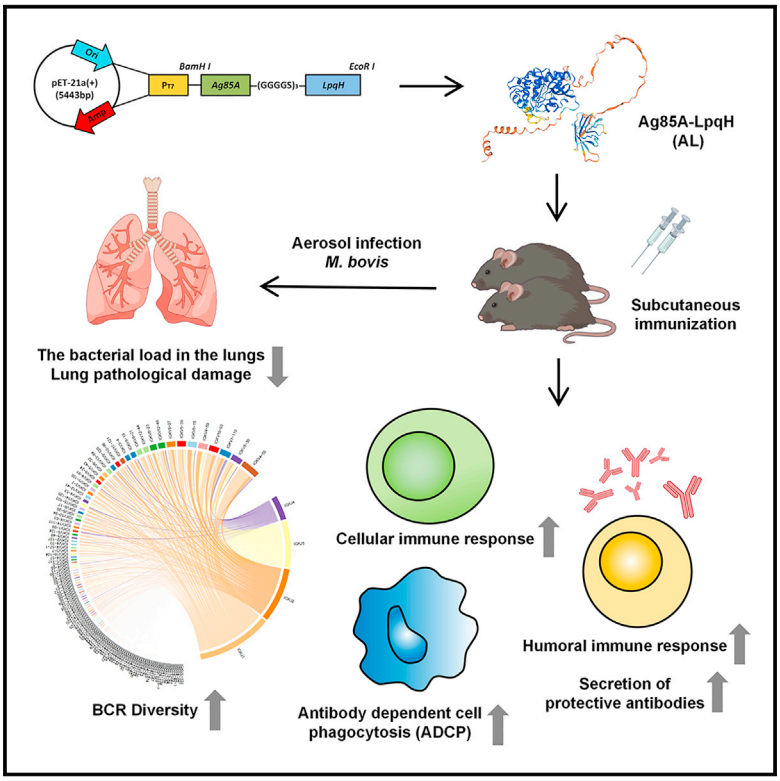

Highlights

- A subunit vaccine Ag85A-LpqH focusing on humoral immunity was designed and constructed
- Ag85A-LpqH can provide significant protection against tuberculosis in mouse infection models
- Ag85A-LpqH can induce robust T cell and B-cell immune responses
- Ag85A-LpqH vaccination on mice can lead to a significant increase in BCR diversity

Authors

Lingyuan Zeng, You Zuo, Minghui Tang, ..., Xiuling Ma, Jiahong Ji, Hao Li

Correspondence

lihao_thu@hotmail.com

In brief

natural sciences, biological sciences, immunology, microbiology

Zeng et al., 2025, iScience *28*, 111568
January 17, 2025
https://doi.org/10.1016/j.isci.2024.111568

CellPress

iScience

CellPress
OPEN ACCESS

Article

A subunit vaccine Ag85A-LpqH focusing on humoral immunity provides substantial protection against tuberculosis in mice

Lingyuan Zeng,[1] You Zuo,[1] Minghui Tang,[1] Chengrui Lei,[1] Huoming Li,[1] Xiuling Ma,[1] Jiahong Ji,[1] and Hao Li[1,2,*]
[1]National Key Laboratory of Veterinary Public Health and Safety, College of Veterinary Medicine, China Agricultural University, Beijing, China
[2]Lead contact
*Correspondence: lihao_thu@hotmail.com
https://doi.org/10.1016/j.isci.2024.111568

SUMMARY

The importance of humoral immunity in combating TB has gained extensive recognition. In this study, a subunit vaccine named Ag85A-LpqH (AL) was prepared by fusing the antigen Ag85A proved to induce robust T cell immune responses, and LpqH was shown to produce protective antibodies. The prevention and BCG prime-boost mouse models were established to test the vaccine efficacy. The results indicate that Ag85A-LpqH can induce substantial protection by reducing bacterial loads and pathological lesions. This vaccine can induce robust antibody responses, as well as T cell immune responses especially strong $CD8^+$ T cell responses. Moreover, the serum from AL-immunized mice can reduce the bacterial load and lung pathology in mice. B cell receptor (BCR) sequencing revealed a notable rise in BCR diversity among mice immunized with AL. These results indicate that Ag85A-LpqH can be a promising vaccine candidate for tuberculosis prevention and control.

INTRODUCTION

Tuberculosis, caused by *Mycobacterium tuberculosis* complex (MTBC), particularly *Mycobacterium tuberculosis* (Mtb) and *Mycobacterium bovis* (*M.bovis*), is one leading cause of death from a single infectious agent around the world. In 2022 around 10 million people became ill with TB, leading to about 1.3 million deaths.[1,2] The emergence of HIV-coinfection and the increase in drug-resistant tuberculosis have presented significant challenges to human tuberculosis control. *M. bovis* can infect both humans and animals. It is estimated that approximately 140,000 TB cases and 11,400 deaths were caused by *M. bovis* infection in 2019. Bovine tuberculosis is distributed globally with significant economic impacts mainly related to livestock production losses and has the potential zoonotic threat.[2,3] Therefore, the One Health approach is essential for controlling zoonotic tuberculosis.

Bacille Calmette-Guérin (BCG) as the only tuberculosis vaccine approved by the World Health Organization (WHO), has been used for over a century. Despite its effectiveness in protecting children, its efficacy in adults varies widely, from 0 to 80%.[4] So it is necessary and urgent to develop novel and effective vaccines to prevent tuberculosis and strengthen the One Health approach. Numerous vaccines have progressed to the clinical stage, such as inactivated vaccines, attenuated vaccines, protein/adjuvant vaccines, viral vector vaccines, and nucleic acid vaccines. Among recombinant subunit vaccines, M72/AS01E (containing Mtb39A and Mtb32A antigens with AS01E adjuvant) has appropriately 50% efficacy for a period up to 3 years after the boost immunization in clinical phase IIb trials.[5,6] These research results allow us to see the dawn of tuberculosis vaccines and the promising potential of recombinant subunit vaccines. Protein/adjuvant vaccines offer stability, safety, and effectiveness, and can selectively combine multiple protective antigens, which can enhance their specificity and immune responses.[7,8] Furthermore, pre-exposure to NTM does not seem to affect the efficacy of non-replicating subunit vaccines which is another advantage for subunit vaccine development.[9,10] In the past several decades, many studies have focused on identifying Mtb antigens inducing T cell immunity, particularly those capable of eliciting $CD4^+$ T cell responses. However, these antigens may not be sufficient to obtain a fully protective immune response against TB.[11] Therefore, some researchers are now dedicated to creating recombinant subunit vaccines that integrate novel antigens such as deficient antigens in BCG compared with Mtb, specific antigens focusing on DC surface receptor, and dominant Mtb antigens at various growth stages, which provide a novel approach to TB vaccine development.[10–17] As tuberculosis research advances, numerous studies have demonstrated the important roles of humoral immunity in tuberculosis infection.[18–24] The antibodies targeting mycobacterial antigens can modify the course of Mycobacteria infection in mice and have protective biological effects.[18–24] Therefore, it is rational to design the subunit vaccines based on the T cells and humoral immunity together.

The Ag85 complex, consisting of Ag85A, Ag85B, and Ag85C, is the primary dominant secreted antigen in Mtb. Ag85A is rich in

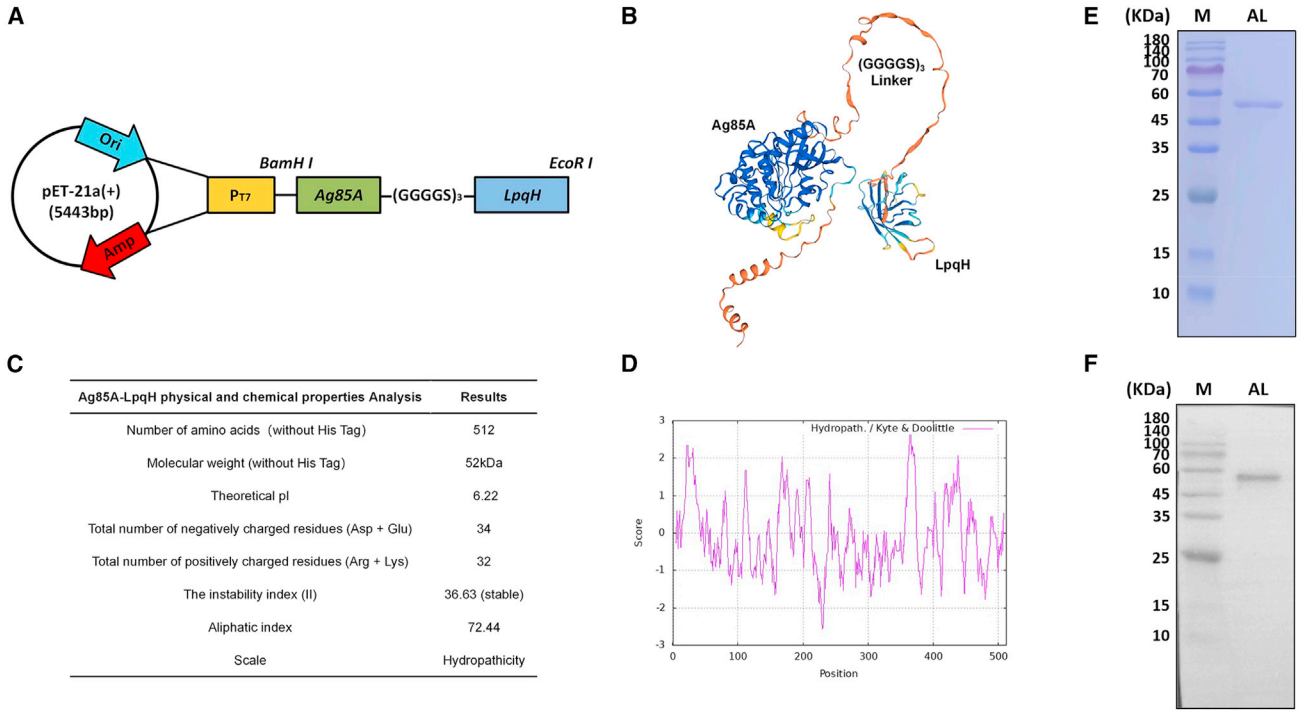

Ag85A-LpqH physical and chemical properties Analysis	Results
Number of amino acids (without His Tag)	512
Molecular weight (without His Tag)	52kDa
Theoretical pI	6.22
Total number of negatively charged residues (Asp + Glu)	34
Total number of positively charged residues (Arg + Lys)	32
The instability index (II)	36.63 (stable)
Aliphatic index	72.44
Scale	Hydropathicity

Figure 1. Ag85A-LpqH structure prediction, expression and identification

(A) The *Ag85A-LpqH* sequence was initially inserted into the pET-21a (+) vector.

(B–D) ExPASy Proteomics Server (www.expasy.org) was utilized for determining the tertiary structure of proteins, as well as predicting the physical and chemical properties of Ag85A-LpqH.

(E and F) Identification of AL was carried out using SDS-PAGE Coomassie Brilliant Blue staining (E) and Western Blot (F), followed by confirmation that the concentration and endotoxin levels met the required standards for further experimentation.

T cell epitopes, facilitating the rapid proliferation of T cells and leading to the production of Th1 cells, thus triggering a robust cellular immune response.[25] Ag85A also plays a crucial role in the survival of Mtb in its dormant state and is essential for maintaining long-term infection.[26] Therefore, Ag85A is regarded as a robust antigen for inducing T cell immunity and is promising for TB vaccine design.[27–29] LpqH, a 19-kDa lipoprotein, is a protein found on the cell wall of Mtb. It primarily functions in the antigen presentation and induction of autophagy via MHC I.[30] LpqH can induce host cells to release TNF-α, IL-6, and other cytokines via the TLR2 and CD14 pathways, thereby boosting the elimination of host cell pathogens.[31,32] Additionally, LpqH can trigger programmed cell death mechanisms such as apoptosis and autophagy to directly eradicate pathogens.[31,32] A recent study has discovered a protective monoclonal antibody against LpqH in an asymptomatic individual, showing the ability of LpqH to provide humoral immune protection against TB.[22] The adjuvants play an important role in novel subunit vaccine development.[33,34] To enhance immunogenicity, lower antigen dosage, achieve precise delivery, and improve antigen interaction with immune cells, the use of adjuvants is necessary for subunit vaccine development.[33,34] In this study, aluminum adjuvant and Poly IC adjuvant were selected as booster adjuvants for the recombinant subunit vaccines Ag85A-LpqH. Aluminum adjuvant is commonly used as a foundational adjuvant, primarily boosting humoral immunity while having a limited ability to stimulate T cell immune responses.[35–37] Moreover, aluminum adjuvants are also crucial in delaying the release of antigens, safeguarding antigen stability, enhancing phagocytosis, and triggering the activation of innate immune cells.[35–37] Poly IC, a synthetic analog of double-stranded RNA, can induce cellular immunity and interferon responses as a TLR3 agonist and can activate antigen-presenting cells (APCs). Furthermore, it can enhance macrophage phagocytosis, repolarize M2 macrophages, and promote the activation of T cells, which is a promising candidate for a vaccine adjuvant against intracellular pathogens.[38–40]

In this study, based on the previous research, we designed and constructed the vaccine candidate Ag85A-LpqH by fusing Ag85A inducing T cells immunity and LpqH with immune-dominant B cell epitopes, and chose aluminum and Poly IC adjuvants as two different vaccine booster to determine the immunogenicity and protective ability of the vaccine candidate Ag85A-LpqH, and the ALA and ALP represent the subunit vaccine Ag85A-LpqH with Alum Adjuvant and poly IC adjuvant separately. The results indicate that Ag85A-LpqH can induce robust T cell and B-cell immunity, and provide significant protection against tuberculosis in mice. These results suggest that it is rational to consider both T and B-cell-mediated immunity when designing TB vaccines, and Ag85A-LpqH could be a promising vaccine for tuberculosis prevention and control.

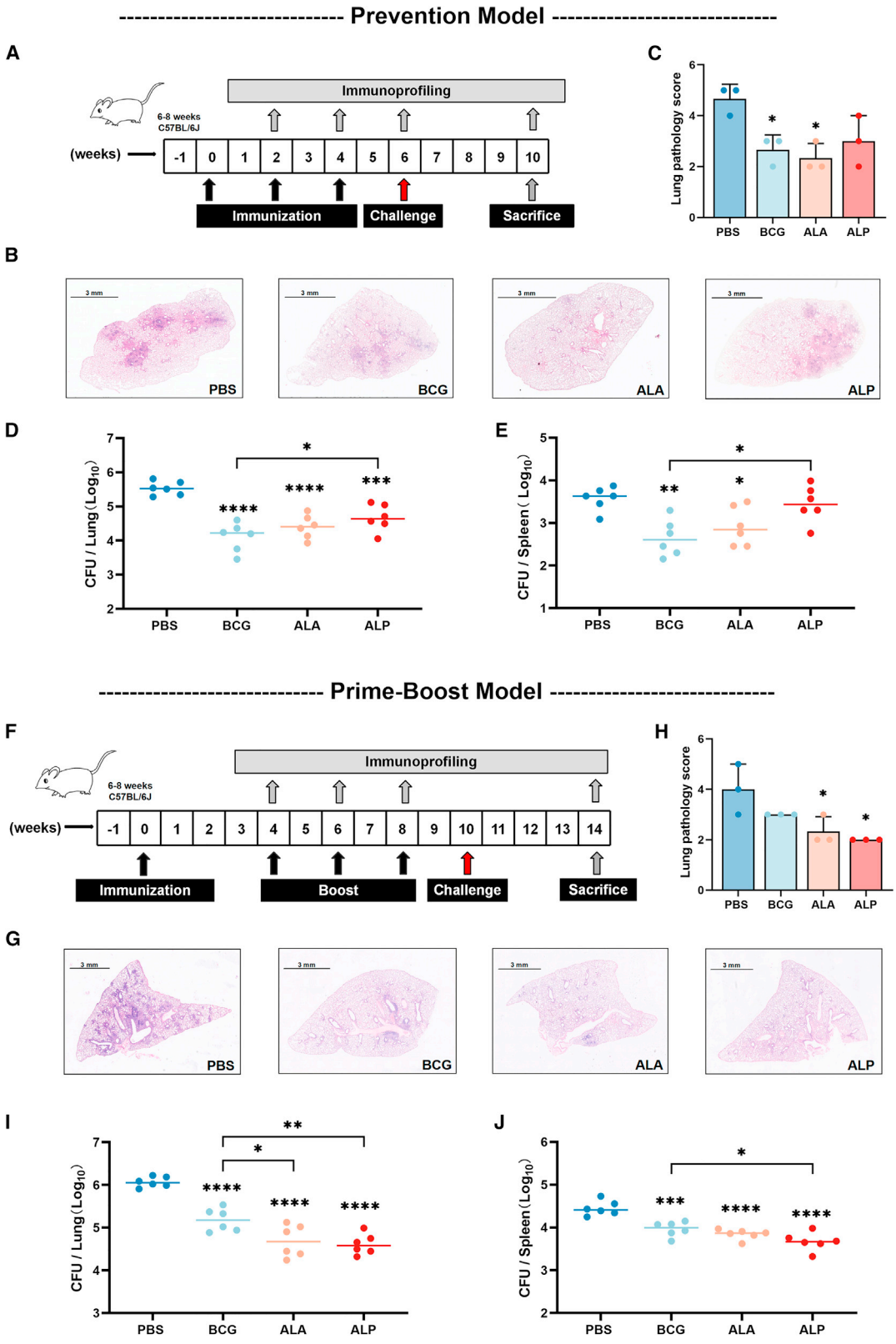

(legend on next page)

RESULTS

Ag85A-LpqH vaccination can provide substantial protection against tuberculosis in mice

Initially, we designed the pET-21a(+)-AL expression vector (Figure 1A). The fusion protein three-dimensional structure was predicted using the Swiss Model (Figure 1B). Expasy ProtParam and Expasy ProtScale were utilized to predict certain physical and chemical properties of Ag85A-LpqH (Figure 1C). The results indicated that the protein is a stable hydrophilic protein with an isoelectric point (pI) of approximately 6.22. Figure 1D displays the total average hydrophilicity (GRAVY) of the Ag85A-LpqH protein across various amino acid sites. Upon confirming the correction of the sequencing, the vector was transferred into BL21 (DE3) for protein expression and purification. The purity and specificity of the protein were confirmed through SDS-PAGE Coomassie Brilliant Blue staining (Figure 1E) and Western Blot (Figure 1F), while the endotoxin level was assessed using the TAL assay. High-quality protein (>95% purity and <10 EU/mL endotoxin level) was then used in subsequent experiments. In this study, the prevention and prime-boost models (Figures 2A and 2F) were used for evaluating the vaccine's efficacy, and the alum and Poly IC were selected as the vaccine adjuvants. In the Prevention model, both the ALA group and the ALP group demonstrated a significant reduction in bacterial load in the lungs of mice post-immunization compared to the PBS group. Additionally, the bacterial load in the spleen was also significantly lower than that in the PBS group for the ALA group. The ALA group exhibited no significant difference in protective effect in the lung and spleen comparable to the BCG group (Figures 2D and 2E). Similarly, in the Prime-Boost model, both the ALA and ALP groups showed a significant decrease in bacterial load in mice lungs compared to the PBS group, with a more pronounced reduction in spleen bacterial load in the ALP group compared to the BCG group (Figures 2I and 2J). Notably, when comparing the ALA and ALP groups using different adjuvants, the ALA group with humoral immune adjuvants displayed superior protective effects in the Prevention model, while the ALP group with cellular immune adjuvants showed better efficacy in the Prime-Boost model. This suggests a potential correlation with the initial immunity conferred by BCG, influencing the body's immune response upon re-immunization. Furthermore, both ALA and ALP groups significantly reduced pathological lung damage in both models, highlighting the protective effects of AL as a vaccine candidate (Figures 2B, 2C, 2G, and 2H).

Ag85A-LpqH vaccination can induce robust humoral immunity in mice

The humoral immunity of mice was assessed by collecting mice serum samples two weeks after each immunization and four weeks post-infection. *M. bovis* strain ELISA was used to analyze different isotypes (IgG, IgM, IgA) and IgG subclasses subtypes (IgG1, IgG2c, IgG3) in mice serum (Figures 3 and 4). In the Prevention model, it was observed that both ALA and ALP mice immunized with different adjuvants showed higher antibody titers, notably the ALA group had significantly higher titers than the BCG and PBS groups after the initial immunization (Figures 3A–3C, and 3E). High Levels of IgG and its subtypes IgG1, IgG2c, and IgG3 in ALA and ALP groups sustained to four weeks post-infection (Figures 3A–3D), while the ALP group displayed relatively lower levels of IgG2c and IgG3 after infection compared to the ALA group (Figures 3C and 3D). In the Prime-Boost model, following the initial booster immunization, there were significantly increasing antibody levels including IgG and its subtypes and IgM in ALA-immunized mice compared to the BCG and PBS group after each immunization (Figure 4). Moreover, high antibody titers were maintained four weeks post-infection in mice (Figure 4). Though ALA IgM had a higher titer after each immunization, this difference disappeared post-infection, indicating that the ALA group could rapidly generate a specific IgG response and shorten the appearance time of the IgM class phase (Figure 4E).

The serum from Ag85A-LpqH-immunized mice exhibited protective effects in mice

In this study, we utilized serum collected from mice four weeks post-infection and co-incubated the serum with BCG and Raw264.7 cells to evaluate the impacts of serum on macrophage phagocytosis of BCG. The flow cytometry analysis indicated that the serum from prevention or prime-boost models can increase macrophage phagocytosis (Figures 5A–5D). Moreover, the CFU counts are consistent with the flow cytometry results (Figures 5A–5D). Though serum from the ALP group also enhances BCG phagocytosis by macrophages, its efficacy is significantly lower in comparison with ALA groups both in the prevention and prime-boost models. Moreover, the serum transfer model was used to assess the protective function of serum antibodies (Figure 5E). Mice were immunized using the Prevention model's immunization program, and serum was collected post-immunization for testing. Each mouse received 300 μL of serum via intraperitoneal injection before infection, followed by 300 CFU of *M. bovis* given to each mouse 5 h later. Two weeks after infection, mice were euthanized for quantifying bacterial loads in the lungs and spleens, as well as evaluating lung pathology. The results indicated that the serum from both the ALA and the BCG groups exhibited a relatively strong protective efficacy on the mice, with the ALA group showing better protection in both the lungs and spleens than the PBS and BCG groups (Figures 5H and 5I). Furthermore, the lung pathology scores in

Figure 2. Ag85A-LpqH protects mice against *M. bovis* infection

(A) Schematic representation of the prevention vaccination schedule.

(B and C) Representative lung pathological changes in the different vaccinations by H&E staining (B). The lung pathological score was evaluated and calculated (C).

(D–J) AL showed a significant reduction in bacterial load in both lungs (D) and spleens (E) of mice infected with *M.bovis*, as well as a notable decrease in pathological damage observed in the lungs (B and C). Similarly, in the Prime-Boost model (F), AL exhibited a significant reduction in bacterial load in the lungs (I) and spleens (J) of mice infected with *M.bovis*, along with a significant decrease in lung pathology (G and H). The scale bar is positioned in the upper-left corner (scale bar length = 3 mm) of the lung tissue sections. Data are represented as mean ± SD. Statistical analyses were performed using one-way ANOVA (ns: not significant; $*p < 0.05$; $**p < 0.01$; $***p < 0.001$; $****p < 0.0001$).

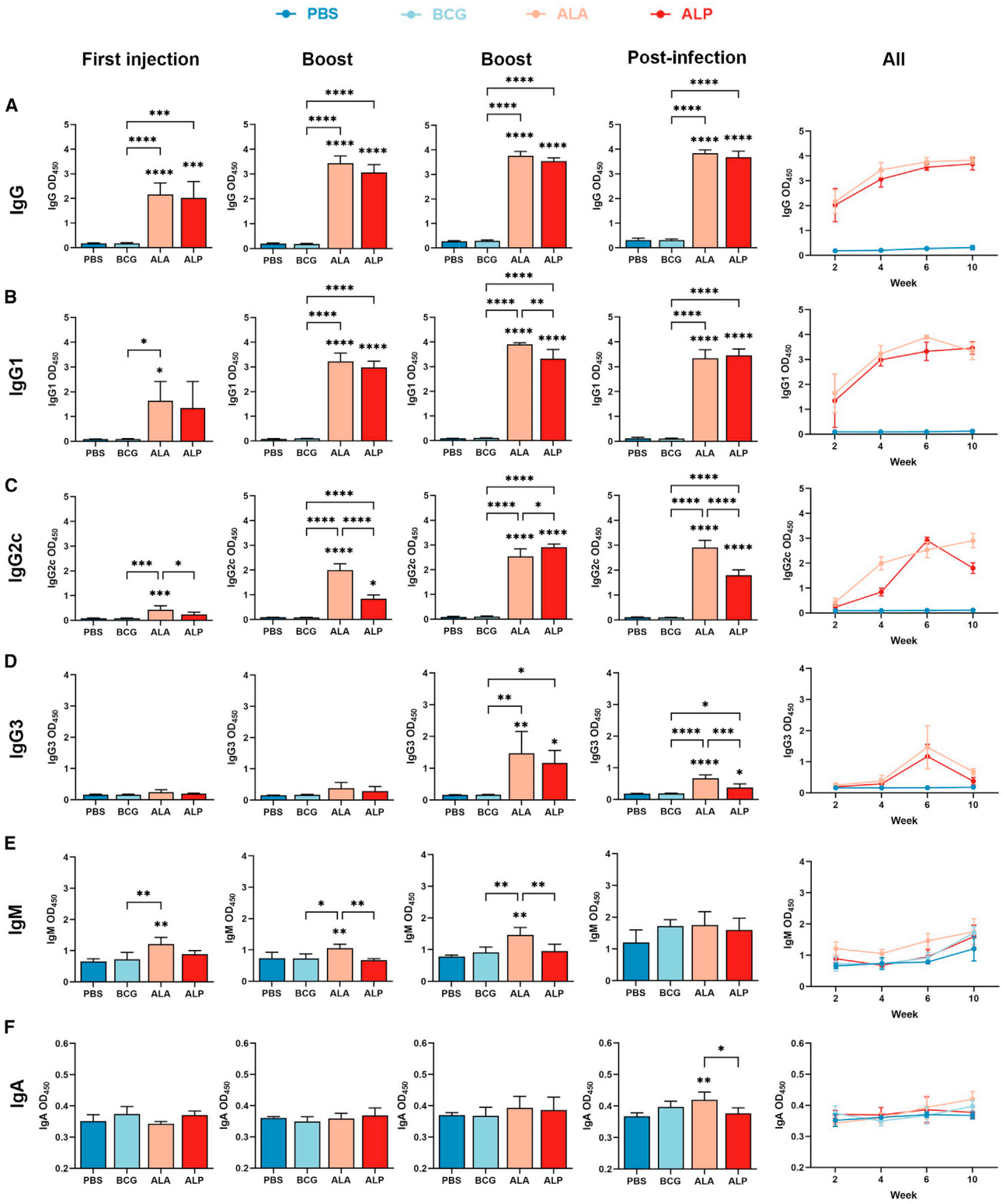

(legend on next page)

the ALA group significantly differed from those of the PBS group (Figures 5F and 5G), suggesting that ALA not only reduced bacterial load in the lungs and spleens but also markedly decreased lung pathology, thereby confirming the protective effects of humoral immunity induced by the ALA vaccination.

Ag85A-LpqH can induce robust cellular immunity

A preliminary assessment of the cellular immune response in mice was conducted by cytokines assay. Spleen lymphocytes were isolated from the mice upon the completion of the immunization program. A single cell suspension of spleen lymphocytes was incubated with 10 μg/mL of specific antigen (Ag85A-LpqH for ALA and ALP groups, BCG lysates for PBS and BCG groups) for 12 h. After incubation, the cytokine levels of IFN-γ, TNF-α, IL-2, IL-17, and IL-10 were measured in the collected supernatant. In the Prevention model, both the ALA and ALP groups exhibited a superior cellular immune response, particularly in IL-2, IL-10, and IL-17 levels, compared to the BCG group (Figure 6A). In the Prime-Boost model, the ALA and ALP groups also demonstrated higher IL-2 levels than the BCG group. Moreover, while the IL-17 level in the ALA group was notably higher compared to the BCG group, its IL-17 level remained at a relatively lower level compared with other cytokines (Figure 6B).

Following immunization in the prevention model, spleen lymphocyte suspension, lymph node single-cell suspension, and bone marrow single-cell suspension were obtained from the PBS, BCG, and ALA groups, respectively. These cells were then incubated with 10 μg/mL BCG lysates (stimulated) or normal medium (non-stimulated) for 12 h. Subsequent analysis showed significant increases in total $CD3^+$ T cell levels, $CD4^+$ T cell levels, and $CD8^+$ T cell levels in the spleen lymphocytes of mice in the ALA group compared to the PBS group in the absence of specific antigen stimulation (Figure 6C). Additionally, the proportion of $CD3^+$ T cells and $CD8^+$ T cells in the ALA group differed significantly from those in the BCG group. Following stimulation, $CD8^+$ T cell levels in the spleen lymphocytes remained significantly higher in the ALA group compared to both the PBS and BCG groups (Figure 6C). Moreover, stimulated lymph node cells exhibited elevated levels of $CD4^+$ and $CD8^+$ T cells (Figure 6D). Dendritic cells (DCs) play a crucial role as antigen-presenting cells. By isolating mice bone marrow cells and assessing DC surface maturity markers, we noted an increase in mature DCs, indicating improved antigen presentation. Particularly, the ALA group exhibited significantly higher proportions of $CD80^+$ DCs and MHC II^+ DCs compared to the PBS group, suggesting a beneficial influence on antigen presentation in the immune response (Figure 6E). The increase in MHC II^+ DCs suggests a potential rise in $CD4^+$ T cells that could be presented to $CD4^+$ T cells. To further investigate this, we induced the differentiation of immature DCs from bone marrow cells of C57BL/6J mice and stimulated them with various antigens for 24 h, then the DCs were co-cultured with spleen lymphocytes at a 1:10 ratio, and the types of spleen lymphocytes were evaluated after 72 h of incubation. The findings indicated that DCs stimulated with AL significantly promoted the differentiation of $CD4^+$ T and $CD8^+$ T spleen lymphocytes, thereby boosting the cellular immune responses (Figure 6F). Spleen lymphocytes from the ALA group showed higher levels of IL-2 and $CD8^+$ T cells in spleen lymphocytes. Given the known correlation between IL-2, an autocrine cytokine, and the increase in $CD8^+$ T cells, we cultured immunized mice spleen lymphocytes with the same concentration of IL-2 for 12 h. The results showed a notable increase in mice spleen $CD8^+$ T lymphocytes, confirming the relationship between IL-2 and $CD8^+$ T cells (Figure 6G).

B cell receptor and T cell receptor repertoires analysis after vaccination

Mice were immunized using the immunization program of the prevention model (Figure 2A). The immunization program consisted of three groups: PBS group (n = 2), BCG group (n = 3), and ALA group (n = 3) (Figure 7A). The initial analysis focused on common indices, revealing a significant decrease in DE50 for the light chains of IGL and IGK, with IGK also showing an increase in singleton (Figures 7B and 7C). These results suggest a high proportion of monoclonal clones in IGL and IGK in mice from the ALA group, indicating potential diverse rearrangements in the light chain. Then the CDR3 diversity of BCR heavy chain, light chain, and TCR heavy chain was analyzed. Results showed that the overall CDR3 diversity of the ALA group was significantly higher than that of the PBS and BCG groups in IGL and IGK (Figure 7D). Individual analysis of samples in different groups also confirmed these findings (Figures 7E–7G), suggesting extensive rearrangements in antibodies post-immunization in the ALA group. Additionally, the TCR heavy chain analysis showed a lower unique amino acid content in the BCG and ALA groups, along with a reduced proportion of monoclonal in these groups (Figures S2A and S2C). Similarly, results can be seen in the related index (Figures S2D–S2F) and the frequency of TCR clone sequences detected once, twice, and three times or more by sequencing (Figure S2B). This indicates that specific antibodies are produced in response to specific antigens, leading to a decrease in random clone proportions. Subsequently, in TCR sequencing, the distribution frequency of the V genes and J genes of the corresponding heavy chain were also analyzed and presented (Figures S2G and S2H).

Next, we analyzed the different subtypes of antibodies produced among these groups (Figures 7H–7P). Figure 7H depicts the ratio between the samples from different groups and the mean value of the negative control group, while Figures 7I–7P show the percentage of different subtypes. Notably, we found that the ALA group exhibited variation in the proportion of IGHG and IGHE, showcasing a superior performance in IGHG1, with

Figure 3. Ag85A-LpqH induces a robust humoral immune response in the prevention mouse model

(A–F) In the Prevention model, blood samples were collected from the tail vein of mice (n = 3∼4) at two weeks after each immunization and four weeks after infection. The samples were stood at 4°C overnight, followed by centrifugation to obtain serum. The serum was then diluted at a ratio of 1:3000 as primary antibodies to detect specific anti-heat-inactivated *M. bovis* total IgG (A), IgG1 (B), IgG2c (C), IgG3 (D), IgM (E), and IgA (F) antibody titers. Each row shows the mice's serum antibody titers after each immunization or sacrifice, and the overall antibody titers change. Data are represented as mean ± SD. Statistical analyses were performed using one-way ANOVA (ns, not significant; $^*p < 0.05$; $^{**}p < 0.01$; $^{***}p < 0.001$; $^{****}p < 0.0001$).

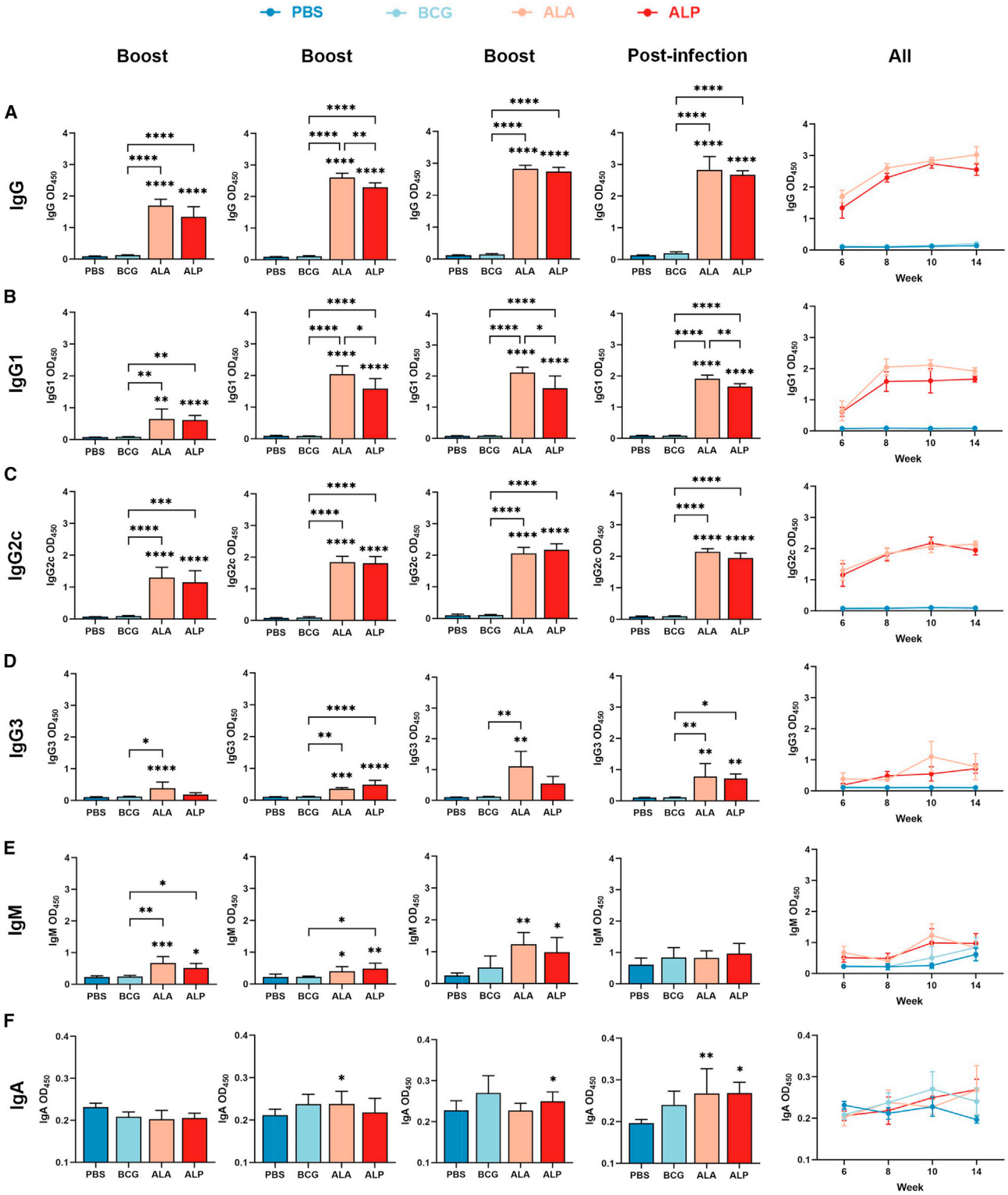

Figure 4. Ag85A-LpqH induces a robust humoral immune response in the Prime-Boost mouse model

In the Prime-Boost animal model, blood samples were collected from the tail vein of mice (n = 3∼4) at two weeks after each booster immunization and four weeks after infection. The samples were then stored at 4°C overnight before undergoing centrifugation to obtain serum. A 1:3000 dilution ratio

(legend continued on next page)

an increase in IGHG2. The observed rise in IGHE could potentially be linked to the increase of $CD8^+$ T cells. Furthermore, owing to the diverse rearrangements of IGK and IGL, an examination of their V-J genes was conducted (Figures 7Q–7T). The analysis revealed distinct expression ratios of V and J genes across the three groups, along with substantial differences in gene combinations (Figures S2I and S2J). In the V-J combination of IGK, the ALA group displayed a preference for IGKJ1 and IGKJ2, while the BCG group favored IGKJ1 and IGKJ5, and the PBS group leaned toward IGKJ2 and IGKJ5. Additionally, the ALA group exhibited a preference for IGKV4-57-1, IGKV5-43, and IGKV6-23, with varying elevations compared to the other groups, potentially indicating its protective properties. Regarding IGL V-J combinations, the ALA group showed higher levels of IGLJ1-IGLV1 and lower levels of IGLJ3-IGLV1 compared to the other groups, which could be associated with its immunogenicity.

DISCUSSION

In this study, we utilized cellular immunity and humoral immunity antigens to develop a novel recombinant subunit fusion vaccine Ag85A-LpqH. Two different adjuvants were used to investigate their potential impact on the vaccine efficacy. The experimental findings revealed that the recombinant subunit vaccine not only induced a robust humoral immune response but also demonstrated significant effects on cellular immunity. Particularly noteworthy is the vaccine's high antibody titers against *M. Bovis*, specifically targeting IgG and its subclasses IgG1, IgG2c, and IgG3. Similarly, results can also be seen in the BCR sequencing, especially the IgG1. Moreover, the candidate exhibited high levels of cytokines such as IFN-γ, IL-2, and IL-10, with a marked increase in IL-17 compared to the BCG group. Ag85A plays an important role in enhancing IL-17 production.[41–43] Ag85A-specific T cells producing the IL-17 were strongly boosted after MVA85A (modified Vaccinia Ankara virus expressing antigen Ag85A) vaccination in both adolescents and children.[41] Furthermore, other studies also suggested that Ag85A is closely related to IL-17 cytokines production in cattle and mice vaccination.[42,43] IL-17 primarily functions to stimulate the production of chemokines and enhance the migration of neutrophils, thus triggering pro-inflammatory responses.[44] While IL-10, known as an anti-inflammatory cytokine, plays a major role in suppressing macrophage and dendritic cell (DC) functions.[45] The upregulation of IL-10 can help balance the Th1/Th2 immune responses.[46–48] Furthermore, IL-10 may be associated with pathological damage in the lungs, the increased levels of IL-10 can help reduce inflammation and alleviate pathological damage in the lungs.[45,49] IL-2, classified as a Th1-type cytokine, serves a crucial function in the proliferation and transformation of T cells.[50] Additionally, it plays a role in regulating the body's immune response, facilitating the generation of antigen-specific $CD8^+$ T cells for enhanced immune reactions, and reversing T cell dysfunction resulting from prolonged stimulation via Mtb.[51,52]

The ALA group showed a substantial increase in IL-2 levels compared to the BCG group, accompanied by a rise in the $CD8^+$ T cell population in the spleen. While $CD4^+$ T cells are commonly believed to have a significant impact on controlling Mtb infection, recent studies have highlighted the crucial role of $CD8^+$ T cells in host defense mechanisms, including the killing of Mtb and the prevention of latent infection.[53,54] Previous studies have demonstrated that IL-2, classified as a Th1 cytokine, can enhance the transition of T cells to $CD8^+$ T cells,[52,55] a correlation further supported by our experimental results. Bone marrow single-cell suspensions were isolated from mice post-immunization. The proportion of mature bone marrow-derived dendritic cells (BMDCs) in the ALA group was significantly higher compared to the PBS group, suggesting that this vaccine enhances BMDCs maturation and aids in antigen presentation. *In vitro* induction of BMDCs with different antigens showed that AL-stimulated BMDCs promoted the differentiation of T cells into $CD4^+$ T cells and $CD8^+$ T cells, particularly $CD8^+$ T cells. These findings suggest that the increase in $CD8^+$ T cells may not solely be due to indirect factors but could also be attributed to direct antigen presentation by dendritic cells. Sequencing the BCR of splenocytes post-immunization showed that the ALA group notably enhanced the diversity of immunoglobulin light chain CDR3 and exhibited a distinct V-J gene combination compared to the BCG and PBS groups. Since the antibody repertoire diversities are correlated to the patient's recovery from virus infection and vaccination protection,[56,57] this supports that AL vaccination in this study may increase antibody diversity and enhance bacteria eradication. The murine antibodies IgG1, IgG3, IgM, and IgA have been shown to be protective against Mtb infection.[20,58] In our study, the AL vaccination can induce robust antibody responses including IgG and its subtypes. The BCR repertoires analysis also indicates that IgG especially IgG1 accounts for more antibody responses compared with BCG and PBS groups, which may suggest that the antibodies' immunity may have important roles in the AL protection against tuberculosis. Moreover. TGB sequencing demonstrated that BCG maintained strong immune properties, facilitating the targeted differentiation of T cells. Though ALA also exhibited this capability, its effectiveness in inducing specific T cells was slightly inferior to BCG. In addition, there are no differences in TCR clonotypes diversity between ALA and BCG, or PBS, which further supports that antibodies may enhance AL vaccination protection.

The experimental results indicate that the protective effects of subunit vaccines with different adjuvants vary across different animal models. This inconsistency is likely due to the specific adjuvants used, as they can influence the immune response in distinct ways. Macrophage phagocytosis results in this study reveal that while the ALP group in mice shows higher antibody titers, it does not enhance the phagocytosis. This highlights the critical role of adjuvants in shaping the immune response bias of vaccines. The findings suggest that selecting an adjuvant

was used as the primary antibody to detect anti-heat-inactivated *M. bovis* IgG (A), IgG1 (B), IgG2c (C), IgG3 (D), IgM (E), and IgA (F) antibody titers. The figure displays the changes in antibody titers two weeks after each boost, four weeks after sacrifice, and the overall antibody titers trends. Data are represented as mean ± SD. Statistical analyses were performed using one-way ANOVA (ns: not significant; $*p < 0.05$; $**p < 0.01$; $***p < 0.001$; $****p < 0.0001$).

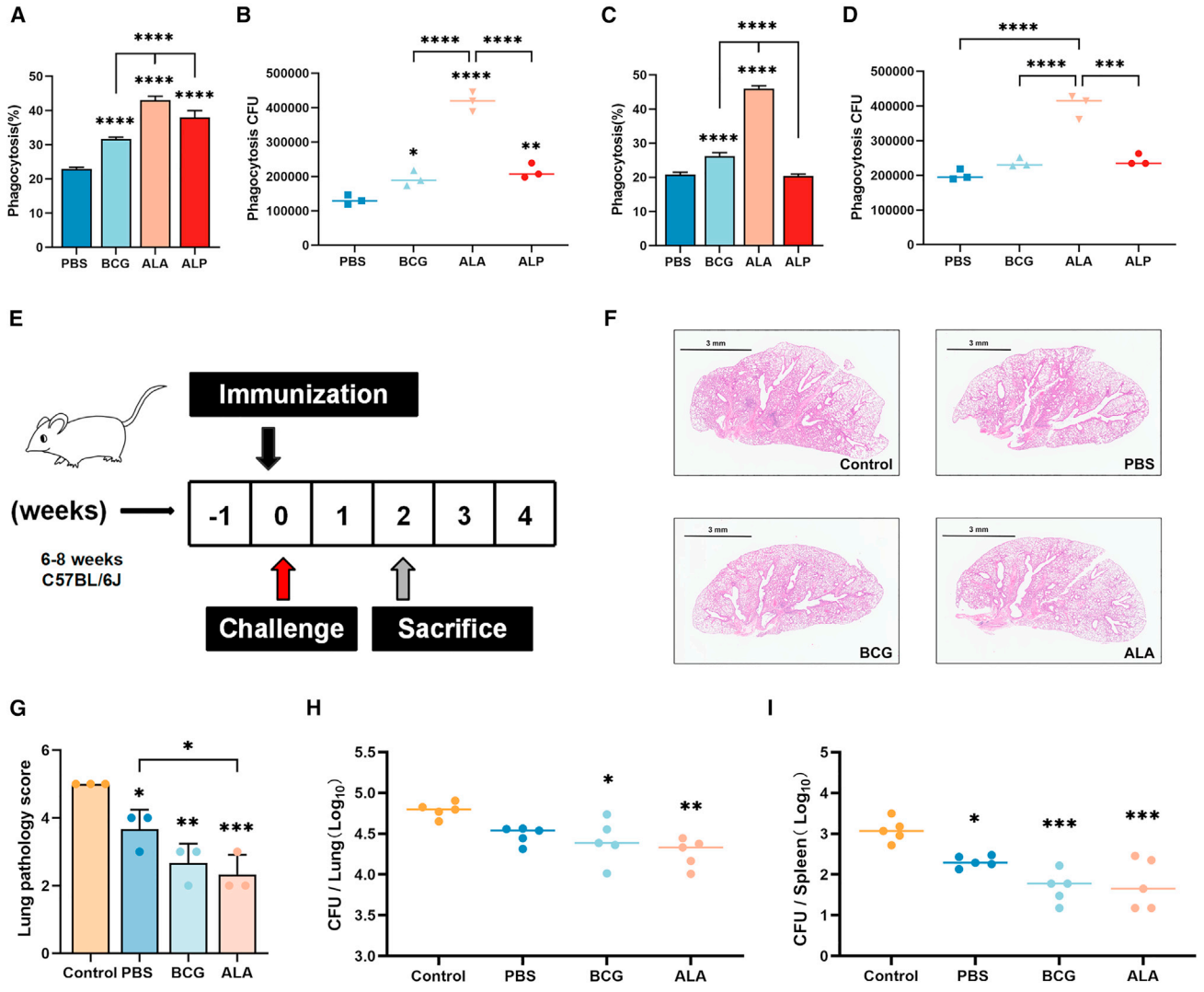

Figure 5. Serum antibodies can increase macrophage phagocytosis and confer improved protection against *M. bovis* infection in mice

(A–D) Sera from mice were collected at the time of sacrifice for cell phagocytosis assays. Initially, FITC-labeled BCG and Raw264.7 cells (MOI = 5:1) were cultured in DMEM medium containing 10% mice serum for 2 h. Following cell washing, fixation with 4% PFA for 2 h, and detection by a BD flow cytometer, the proportion of cells phagocytosing BCG was analyzed in the Prevention Model (A) and Prime-Boost Model (C). Subsequently, a macrophage phagocytosis assay based on CFU counts was utilized to enumerate the number of phagocytosed bacteria. Raw264.7 cells were infected with BCG at MOI = 5 for 2 h in a medium with 10% mouse serum. After washing, cell lysis, dilution, and plating were performed to quantify the number of phagocytosed bacteria in the Prevention Model (B) and Prime-Boost Model (D).

(E–I) The functionality of mice immunized serum was investigated on animals in this study. The immunized mice serum was harvested in the Prevention Model, and the serum transfer animal model (E) was used to determine if the mice serum could effectively decrease the risk of post-infection. The study analyzed the bacterial load in the lungs (H) and spleen (I) of mice, as well as the impact of the serum on pathological damage to mice lungs (F and G). The scale bar is positioned in the upper-left corner (scale bar length = 3 mm) of the lung tissue sections. Control group: the mice injected with PBS; PBS group: the mice injected with serum from mice immunized with PBS; BCG group: the mice injected with serum from mice immunized with BCG; ALA group: the mice injected with serum from mice immunized with ALA. Data are represented as mean ± SD. Statistical analyses were performed using one-way ANOVA (ns: not significant; $^{*}p < 0.05$; $^{**}p < 0.01$; $^{***}p < 0.001$; $^{****}p < 0.0001$).

that favors humoral immune response is essential for promoting experiential immunity. Groups using the same vaccine and adjuvant exhibited inconsistent protective effects in different animal models, despite all significantly reducing bacterial load in lungs and lung pathology. We hypothesized that this inconsistency may be due to BCG priming immunity in the Prime-Boost model. The initial BCG immunization could potentially bias the immune response of mice, leading to more rapid cellular immune responses upon booster immunization. In the Prevention model, the ALA group demonstrated superior cellular and humoral immune responses. Therefore, we suggest that to better showcase the protective efficacy of the recombinant subunit vaccine with humoral immune fusion antigens, utilizing a model without prior BCG vaccination may be more effective.

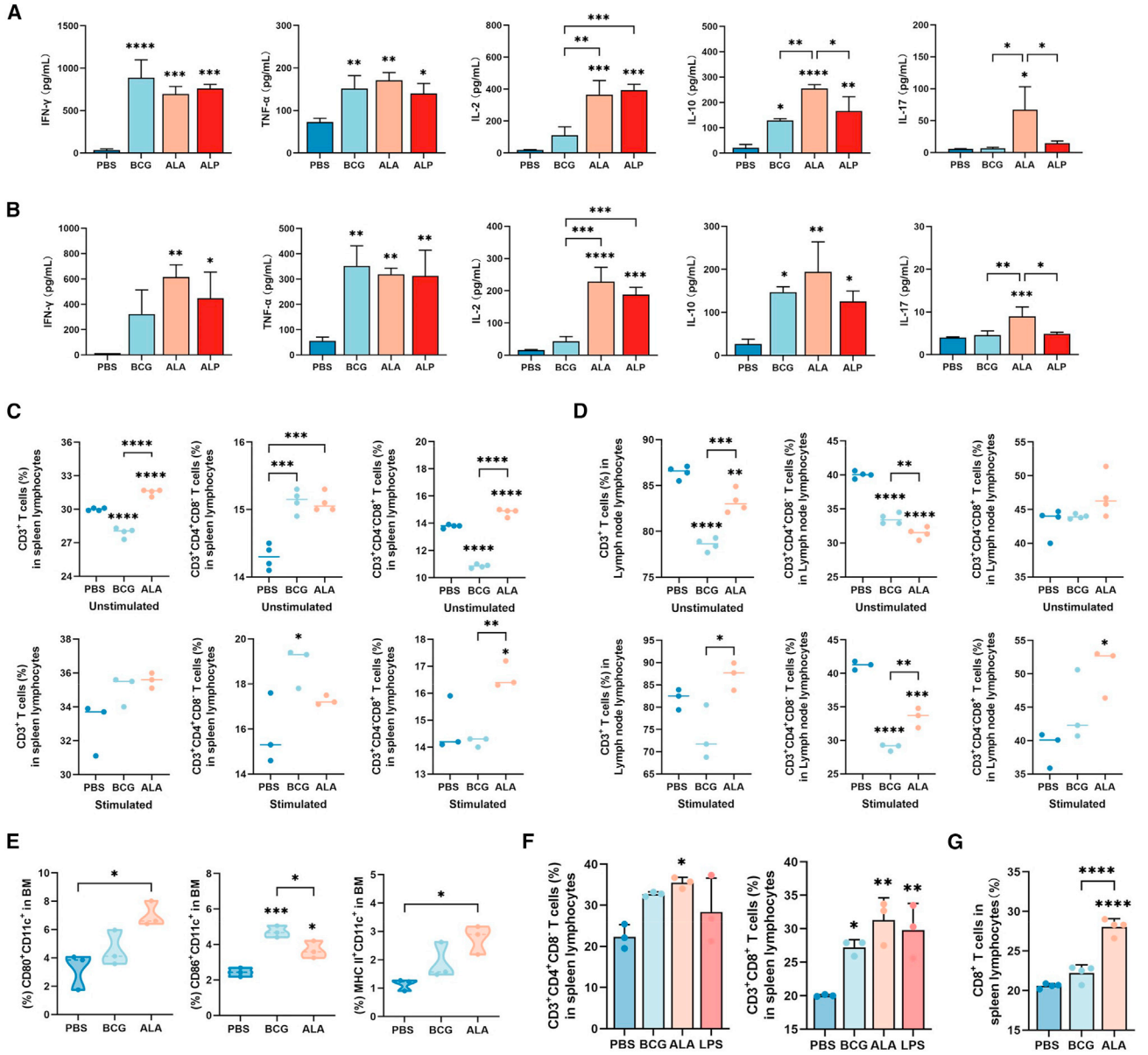

Figure 6. Ag85A-LpqH vaccination can induce robust cellular immunity in mice

(A and B) Two weeks post the final immunization. Mice spleens were collected to harvest single-cell suspensions. These cells were then stimulated with specific antigens for 12 h, followed by centrifugation. The cell supernatants were used to detect cytokines secreted by the cells in the Prevention Model (A) and Prime-Boost model (B). Two weeks after the last immunization, single-cell suspensions from the spleens and lymph nodes of the mice were obtained. These cells were then stimulated for 12 h using BCG lysis buffer, followed by centrifugation, staining of the cell pellet, and analysis of $CD3^+$ T, $CD4^+$ T, and $CD8^+$ T cell populations in the spleen cells (C) and lymph node cells (D) when stimulated and unstimulated by BCG lysate to observe changes in cell proportions. Furthermore, bone marrow cells were isolated to assess BMDC maturation (E). To delve deeper into the influence of mature BMDCs on cell presentation, BMDCs were isolated and induced *in vitro*. After stimulation with different antigens to promote maturation, these BMDCs were co-incubated with spleen lymphocytes at a ratio of 1:10 to study the presentation of mature BMDCs to T cells (F). In the Prevention Model, single splenocyte suspensions from mice two weeks after the last immunization were incubated with IL-2 for 12 h to assess the impact of IL-2 on $CD8^+$ T cells in different groups (G). Data are represented as mean ± SD. Statistical analyses were performed using one-way ANOVA (ns, not significant; $^*p < 0.05$; $^{**}p < 0.01$; $^{***}p < 0.001$; $^{****}p < 0.0001$).

In this study, we combined humoral immune antigens with cellular immune antigens to develop a recombinant subunit vaccine that can elicit both cellular and humoral immune responses. This vaccine not only boosts immunity levels post-immunization but also maintains antibody titers post-infection. Furthermore, the serum from infected mice in the vaccine group enhances the phagocytosis. In animal models, the serum from mice in the vaccinated group reduces bacterial load in the lungs and spleens of infected mice, as well as mitigates lung damage lesions. These findings support the efficacy of recombinant

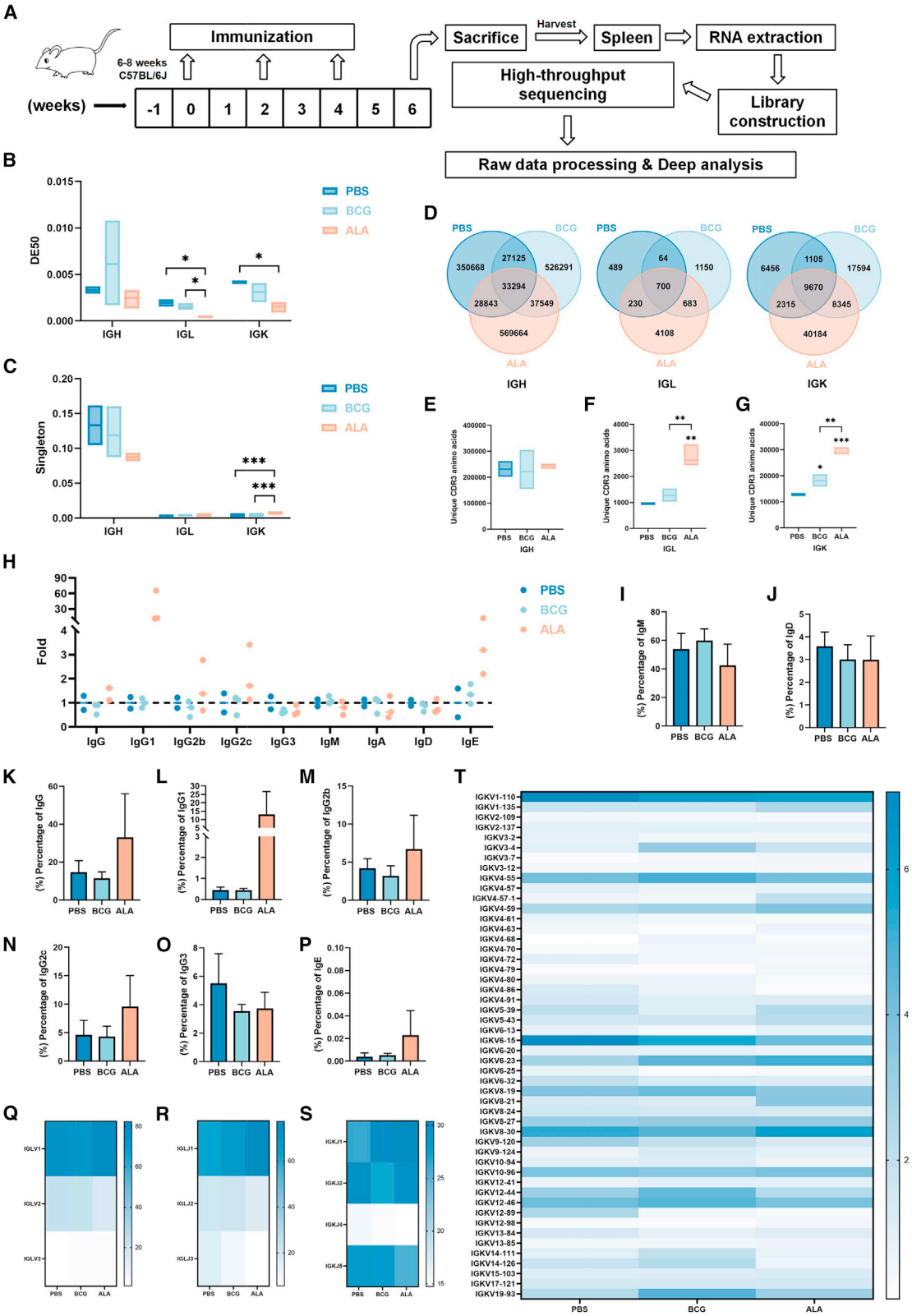

(legend on next page)

subunit vaccines incorporating humoral immune antigens for protective immunity. However, the use of adjuvants should be carefully considered to optimize humoral immunity. In the future, when incorporating multiple antigens in vaccines, it is crucial to balance and coordinate humoral and cellular immune antigens to maintain a robust immune response and effectively stimulate both humoral and cellular immunity. Above all, our research introduces a novel approach for developing recombinant subunit vaccines fused with humoral immune antigens, identifies an appropriate model for humoral immune antigens, and offers fresh insights for tuberculosis vaccine development.

Limitations of the study

In this study, the virulent *M. bovis* strain was used as the challenge strain for female C57BL/6J mice to establish the prevention and prime-boost models. It will be important to investigate the protective effects of Ag85A-LpqH on additional mouse strains such as BALB/c and heterologous challenge strains such as H37Rv. All the mice used in this study are female, therefore, it is better to perform the challenge experiments on male mice, since we do not know whether the sex can affect the mice's susceptibility and disease progression to *M. bovis* infection. Additional mice infection models such as ultra-low dose infection models and long-term protection models will also be considered in future studies to investigate the vaccine's efficacy.

RESOURCE AVAILABILITY

Lead contact

Further information and requests for resources should be directed to and will be fulfilled by the lead contact, Hao Li (lihao_thu@hotmail.com).

Materials availability

This study did not generate new unique reagents.

Data and code availability

- All data reported in this article will be shared by the lead contact upon request. All original sequencing data have been uploaded to the NCBI SRA (Sequence Read Archive). Accession numbers are listed on the key resources table.
- This article does not report the original code.
- Any additional information needed to reanalyze the data reported in this article is available from the lead contact upon request.

ACKNOWLEDGMENTS

We thank China Agricultural University for providing the flow cytometry, confocal microscopy, and biosafety facilities that allowed us to conduct this study. We thank ImmuQuad Biotech for their help in deep sequencing and data analysis. We thank Prof. Babak Javid for helpful discussions on this work. This work was supported by The National Natural Science Foundation of China (Project No. 32070937); The National Key Research and Development Program (Project No. 2021YFD1800405); and the 2115 Talent Development Program of China Agricultural University (00109029).

AUTHOR CONTRIBUTIONS

H. Li conceived the study, directed the research and acquired funding. H. Li and L. Zeng designed the experiments. L. Zeng performed the experiments and analyzed the data. Y. Zuo, M. Tang, C. Lei, H. Li, X. Ma and J. Ji assisted with the experiments. H. Li and L. Zeng wrote the article.

DECLARATION OF INTERESTS

The authors declare that there are no conflicts of interest.

STAR★METHODS

Detailed methods are provided in the online version of this paper and include the following:

- KEY RESOURCES TABLE
- EXPERIMENTAL MODEL AND STUDY PARTICIPANT DETAILS
  - Ethics statements
  - Bacterial culture
  - Cell lines
  - Mice
- METHOD DETAILS
  - Preparation of the Ag85A-LpqH
  - Mouse challenge models
  - Histopathological analysis
  - Enzyme-linked immunosorbent assay (ELISA)
  - Preparation of single-cell suspensions
  - Cytokines detection assay
  - Cell analysis by flow cytometry
  - Mixed lymphocyte reaction assay
  - Macrophage phagocytosis assay
  - BCR and TCR repertoires sequencing and analysis
- QUANTIFICATION AND STATISTICAL ANALYSIS

SUPPLEMENTAL INFORMATION

Supplemental information can be found online at https://doi.org/10.1016/j.isci.2024.111568.

Received: August 23, 2024
Revised: October 4, 2024
Accepted: December 6, 2024
Published: December 20, 2024

REFERENCES

1. WHO (2023). Global tuberculosis report.
2. Müller, B., Durr, S., Alonso, S., Hattendorf, J., Laisse, C.J., Parsons, S.D., van Helden, P.D., and Zinsstag, J. (2013). Zoonotic Mycobacterium bovis-

Figure 7. BCR and TCR repertoires analysis after Ag85A-LpqH vaccination in mice

(A) Mice in different groups were immunized with the protocol of the Prevention Model. Following two weeks post-final immunization, spleens were collected, and the spleen single-cell suspensions were separated for RNA extraction. Subsequently, TCR and BCR sequencing was conducted on the machine after passing quality inspection.

(B and C) Various related indices were analyzed, with differences observed in the DE50 index (B) and Singleton index (C). A comprehensive summary analysis of all unique amino acids was carried out (D). Unique amino acids in the CDR3 region of the BCR heavy chain IGH (E), as well as the two light chains IGL (F) and IGK (G) were analyzed.

(H–P) the antibody subtypes of BCR were analyzed. Notably, the two light chains of IGK and IGL exhibited relatively rich diversity, leading to the analysis of IGL-V Gene (Q), IGL-J Gene (R), IGK-J Gene (S), and IGK-V Gene (T). Data are represented as mean ± SD. Statistical analyses were performed using one-way ANOVA (ns: not significant; $*p < 0.05$; $**p < 0.01$; $***p < 0.001$).

induced tuberculosis in humans. Emerg. Infect. Dis. *19*, 899–908. https://doi.org/10.3201/eid1906.120543.

3. Cox, H., Salaam-Dreyer, Z., Goig, G.A., Nicol, M.P., Menardo, F., Dippenaar, A., Mohr-Holland, E., Daniels, J., Cudahy, P.G.T., Borrell, S., et al. (2021). Potential contribution of HIV during first-line tuberculosis treatment to subsequent rifampicin-monoresistant tuberculosis and acquired tuberculosis drug resistance in South Africa: a retrospective molecular epidemiology study. Lancet. Microbe *2*, e584–e593. https://doi.org/10.1016/S2666-5247(21)00144-0.
4. Qu, M., Zhou, X., and Li, H. (2021). BCG vaccination strategies against tuberculosis: updates and perspectives. Hum. Vaccines Immunother. *17*, 5284–5295. https://doi.org/10.1080/21645515.2021.2007711.
5. Van der Meeren, O., Hatherill, M., Nduba, V., Wilkinson, R.J., Muyoyeta, M., Van Brakel, E., Ayles, H.M., Henostroza, G., Thienemann, F., Scriba, T.J., et al. (2018). Phase 2b Controlled Trial of M72/AS01 Vaccine to Prevent Tuberculosis. N. Engl. J. Med. *379*, 1621–1634. https://doi.org/10.1056/NEJMoa1803484.
6. Tait, D.R., Hatherill, M., Van Der Meeren, O., Ginsberg, A.M., Van Brakel, E., Salaun, B., Scriba, T.J., Akite, E.J., Ayles, H.M., Bollaerts, A., et al. (2019). Final Analysis of a Trial of M72/AS01 Vaccine to Prevent Tuberculosis. N. Engl. J. Med. *381*, 2429–2439. https://doi.org/10.1056/NEJMoa1909953.
7. Mascola, J.R., and Fauci, A.S. (2020). Novel vaccine technologies for the 21st century. Nat. Rev. Immunol. *20*, 87–88. https://doi.org/10.1038/s41577-019-0243-3.
8. Zhang, Y., Xu, J.C., Hu, Z.D., and Fan, X.Y. (2023). Advances in protein subunit vaccines against tuberculosis. Front. Immunol. *14*, 1238586. https://doi.org/10.3389/fimmu.2023.1238586.
9. Brandt, L., Feino Cunha, J., Weinreich Olsen, A., Chilima, B., Hirsch, P., Appelberg, R., and Andersen, P. (2002). Failure of the Mycobacterium bovis BCG vaccine: some species of environmental mycobacteria block multiplication of BCG and induction of protective immunity to tuberculosis. Infect. Immun. *70*, 672–678. https://doi.org/10.1128/IAI.70.2.672-678.2002.
10. Woodworth, J.S., Clemmensen, H.S., Battey, H., Dijkman, K., Lindenstrøm, T., Laureano, R.S., Taplitz, R., Morgan, J., Aagaard, C., Rosenkrands, I., et al. (2021). A Mycobacterium tuberculosis-specific subunit vaccine that provides synergistic immunity upon co-administration with Bacillus Calmette-Guerin. Nat. Commun. *12*, 6658. https://doi.org/10.1038/s41467-021-26934-0.
11. Steigler, P., Verrall, A.J., and Kirman, J.R. (2019). Beyond memory T cells: mechanisms of protective immunity to tuberculosis infection. Immunol. Cell Biol. *97*, 647–655. https://doi.org/10.1111/imcb.12278.
12. Andersen, P., and Scriba, T.J. (2019). Moving tuberculosis vaccines from theory to practice. Nat. Rev. Immunol. *19*, 550–562. https://doi.org/10.1038/s41577-019-0174-z.
13. Khademi, F., Derakhshan, M., Yousefi-Avarvand, A., Tafaghodi, M., and Soleimanpour, S. (2018). Multi-stage subunit vaccines against *Mycobacterium tuberculosis*: an alternative to the BCG vaccine or a BCG-prime boost? Expert Rev. Vaccines *17*, 31–44. https://doi.org/10.1080/14760584.2018.1406309.
14. Schrager, L.K., Chandrasekaran, P., Fritzell, B.H., Hatherill, M., Lambert, P.H., McShane, H., Tornieporth, N., and Vekemans, J. (2018). WHO preferred product characteristics for new vaccines against tuberculosis. Lancet Infect. Dis. *18*, 828–829. https://doi.org/10.1016/S1473-3099(18)30421-3.
15. Stylianou, E., Harrington-Kandt, R., Beglov, J., Bull, N., Pinpathomrat, N., Swarbrick, G.M., Lewinsohn, D.A., Lewinsohn, D.M., and McShane, H. (2018). Identification and Evaluation of Novel Protective Antigens for the Development of a Candidate Tuberculosis Subunit Vaccine. Infect. Immunol. *86*, e00014-18. https://doi.org/10.1128/IAI.00014-18.
16. Velasquez, L.N., Stüve, P., Gentilini, M.V., Swallow, M., Bartel, J., Lycke, N.Y., Barkan, D., Martina, M., Lujan, H.D., Kalay, H., et al. (2018). Targeting Antigens to Dendritic Cells the DC-Specific-ICAM3-Grabbing-Nonintegrin Receptor Induces Strong T-Helper 1 Immune Responses. Front. Immunol. *9*, 471. https://doi.org/10.3389/fimmu.2018.00471.
17. Voss, G., Casimiro, D., Neyrolles, O., Williams, A., Kaufmann, S.H.E., McShane, H., Hatherill, M., and Fletcher, H.A. (2018). Progress and challenges in TB vaccine development. F1000Res. *7*, 199. https://doi.org/10.12688/f1000research.13588.1.
18. Phuah, J., Wong, E.A., Gideon, H.P., Maiello, P., Coleman, M.T., Hendricks, M.R., Ruden, R., Cirrincione, L.R., Chan, J., Lin, P.L., and Flynn, J.L. (2016). Effects of B Cell Depletion on Early Infection in Cynomolgus Macaques. Infect. Immun. *84*, 1301–1311. https://doi.org/10.1128/IAI.00083-16.
19. Maglione, P.J., Xu, J., and Chan, J. (2007). B cells moderate inflammatory progression and enhance bacterial containment upon pulmonary challenge with. J. Immunol. *178*, 7222–7234. https://doi.org/10.4049/jimmunol.178.11.7222.
20. Li, H., and Javid, B. (2018). Antibodies and tuberculosis: finally coming of age? Nat. Rev. Immunol. *18*, 591–596. https://doi.org/10.1038/s41577-018-0028-0.
21. Li, H., Wang, X.X., Wang, B., Fu, L., Liu, G., Lu, Y., Cao, M., Huang, H., and Javid, B. (2017). Latently and uninfected healthcare workers exposed to TB make protective antibodies against. Proc. Natl. Acad. Sci. USA *114*, 5023–5028. https://doi.org/10.1073/pnas.1611776114.
22. Krishnananthasivam, S., Li, H., Bouzeyen, R., Shunmuganathan, B., Purushotorman, K., Liao, X., Du, F., Friis, C.G.K., Crawshay-Williams, F., Boon, L.H., et al. (2023). An anti-LpqH human monoclonal antibody from an asymptomatic individual mediates protection against Mycobacterium tuberculosis. NPJ Vaccines *8*, 127. https://doi.org/10.1038/s41541-023-00710-1.
23. Lu, L.L., Chung, A.W., Rosebrock, T.R., Ghebremichael, M., Yu, W.H., Grace, P.S., Schoen, M.K., Tafesse, F., Martin, C., Leung, V., et al. (2016). A Functional Role for Antibodies in Tuberculosis. Cell *167*, 433–443.e14. https://doi.org/10.1016/j.cell.2016.08.072.
24. Watson, A., Li, H., Ma, B., Weiss, R., Bendayan, D., Abramovitz, L., Ben-Shalom, N., Mor, M., Pinko, E., Bar Oz, M., et al. (2021). Human antibodies targeting a Mycobacterium transporter protein mediate protection against tuberculosis. Nat. Commun. *12*, 602. https://doi.org/10.1038/s41467-021-20930-0.
25. Babaki, M.K.Z., Soleimanpour, S., and Rezaee, S.A. (2017). Antigen 85 complex as a powerful immunogene: Biology, immune-pathogenicity, applications in diagnosis, and vaccine design. Microb. Pathog. *112*, 20–29. https://doi.org/10.1016/j.micpath.2017.08.040.
26. Elamin, A.A., Stehr, M., Spallek, R., Rohde, M., and Singh, M. (2011). The Ag85A is a novel diacylglycerol acyltransferase involved in lipid body formation. Mol. Microbiol. *81*, 1577–1592. https://doi.org/10.1111/j.1365-2958.2011.07792.x.
27. Manjaly Thomas, Z.R., Satti, I., Marshall, J.L., Harris, S.A., Lopez Ramon, R., Hamidi, A., Minhinnick, A., Riste, M., Stockdale, L., Lawrie, A.M., et al. (2019). Alternate aerosol and systemic immunisation with a recombinant viral vector for tuberculosis, MVA85A: A phase I randomised controlled trial. PLoS Med. *16*, e1002790. https://doi.org/10.1371/journal.pmed.1002790.
28. Pathan, A.A., Minassian, A.M., Sander, C.R., Rowland, R., Porter, D.W., Poulton, I.D., Hill, A.V.S., Fletcher, H.A., and McShane, H. (2012). Effect of vaccine dose on the safety and immunogenicity of a candidate TB vaccine, MVA85A, in BCG vaccinated UK adults. Vaccine *30*, 5616–5624. https://doi.org/10.1016/j.vaccine.2012.06.084.
29. Dintwe, O.B., Day, C.L., Smit, E., Nemes, E., Gray, C., Tameris, M., McShane, H., Mahomed, H., Hanekom, W.A., and Scriba, T.J. (2013). Heterologous vaccination against human tuberculosis modulates antigen-specific CD4+ T-cell function. Eur. J. Immunol. *43*, 2409–2420. https://doi.org/10.1002/eji.201343454.
30. Hu, D., Wu, J., Zhang, R., Chen, L., Chen, Z., Wang, X., Xu, L., Xiao, J., Hu, F., and Wu, C. (2014). Autophagy-targeted vaccine of LC3-LpqH DNA and

its protective immunity in a murine model of tuberculosis. Vaccine *32*, 2308–2314. https://doi.org/10.1016/j.vaccine.2014.02.069.

31. López, M., Sly, L.M., Luu, Y., Young, D., Cooper, H., and Reiner, N.E. (2003). The 19-kDa protein induces macrophage apoptosis through toll-like receptor-2. J. Immunol. *170*, 2409–2416. https://doi.org/10.4049/jimmunol.170.5.2409.
32. Shin, D.M., Yuk, J.M., Lee, H.M., Lee, S.H., Son, J.W., Harding, C.V., Kim, J.M., Modlin, R.L., and Jo, E.K. (2010). Mycobacterial lipoprotein activates autophagy via TLR2/1/CD14 and a functional vitamin D receptor signalling. Cell Microbiol. *12*, 1648–1665. https://doi.org/10.1111/j.1462-5822.2010.01497.x.
33. Zhao, T., Cai, Y., Jiang, Y., He, X., Wei, Y., Yu, Y., and Tian, X. (2023). Vaccine adjuvants: mechanisms and platforms. Signal Transduct. Targeted Ther. *8*, 283. https://doi.org/10.1038/s41392-023-01557-7.
34. Duong, V.T., Skwarczynski, M., and Toth, I. (2023). Towards the development of subunit vaccines against tuberculosis: The key role of adjuvant. Tuberculosis *139*, 102307. https://doi.org/10.1016/j.tube.2023.102307.
35. Peng, S., Cao, F., Xia, Y., Gao, X.D., Dai, L., Yan, J., and Ma, G. (2020). Particulate Alum via Pickering Emulsion for an Enhanced COVID-19 Vaccine Adjuvant. Adv. Mater. *32*, e2004210. https://doi.org/10.1002/adma.202004210.
36. HogenEsch, H., O'Hagan, D.T., and Fox, C.B. (2018). Optimizing the utilization of aluminum adjuvants in vaccines: you might just get what you want. NPJ Vaccines *3*, 51. https://doi.org/10.1038/s41541-018-0089-x.
37. Moreno-Mendieta, S.A., Rocha-Zavaleta, L., and Rodriguez-Sanoja, R. (2010). Adjuvants in tuberculosis vaccine development. FEMS Immunol. Med. Microbiol. *58*, 75–84. https://doi.org/10.1111/j.1574-695X.2009.00629.x.
38. Alexopoulou, L., Holt, A.C., Medzhitov, R., and Flavell, R.A. (2001). Recognition of double-stranded RNA and activation of NF-κB by Toll-like receptor 3. Nature *413*, 732–738. https://doi.org/10.1038/35099560.
39. Martins, K.A.O., Bavari, S., and Salazar, A.M. (2015). Vaccine adjuvant uses of poly-IC and derivatives. Expert Rev. Vaccines *14*, 447–459. https://doi.org/10.1586/14760584.2015.966085.
40. Stahl-Hennig, C., Eisenblätter, M., Jasny, E., Rzehak, T., Tenner-Racz, K., Trumpfheller, C., Salazar, A.M., Überla, K., Nieto, K., Kleinschmidt, J., et al. (2009). Synthetic Double-Stranded RNAs Are Adjuvants for the Induction of T Helper 1 and Humoral Immune Responses to Human Papillomavirus in Rhesus Macaques. PLoS Pathog. *5*, e1000373. https://doi.org/10.1371/journal.ppat.1000373.
41. Scriba, T.J., Tameris, M., Mansoor, N., Smit, E., van der Merwe, L., Isaacs, F., Keyser, A., Moyo, S., Brittain, N., Lawrie, A., et al. (2010). Modified vaccinia Ankara-expressing Ag85A, a novel tuberculosis vaccine, is safe in adolescents and children, and induces polyfunctional CD4+ T cells. Eur. J. Immunol. *40*, 279–290. https://doi.org/10.1002/eji.200939754.
42. Vordermeier, H.M., Villarreal-Ramos, B., Cockle, P.J., McAulay, M., Rhodes, S.G., Thacker, T., Gilbert, S.C., McShane, H., Hill, A.V.S., Xing, Z., and Hewinson, R.G. (2009). Viral booster vaccines improve Mycobacterium bovis BCG-induced protection against bovine tuberculosis. Infect. Immun. *77*, 3364–3373. https://doi.org/10.1128/IAI.00287-09.
43. Hu, Z., Xia, J., Wu, J., Zhao, H., Ji, P., Gu, L., Gu, W., Chen, Z., Xu, J., Huang, X., et al. (2024). A multistage Sendai virus vaccine incorporating latency-associated antigens induces protection against acute and latent tuberculosis. Emerg. Microb. Infect. *13*, 2300463. https://doi.org/10.1080/22221751.2023.2300463.
44. Seiler, P., Aichele, P., Bandermann, S., Hauser, A.E., Lu, B., Gerard, N.P., Gerard, C., Ehlers, S., Mollenkopf, H.J., and Kaufmann, S.H.E. (2003). Early granuloma formation after aerosol infection is regulated by neutrophils via CXCR3-signaling chemokines. Eur. J. Immunol. *33*, 2676–2686. https://doi.org/10.1002/eji.200323956.
45. Redford, P.S., Murray, P.J., and O'Garra, A. (2011). The role of IL-10 in immune regulation during M. tuberculosis infection. Mucosal Immunol. *4*, 261–270. https://doi.org/10.1038/mi.2011.7.
46. Bashyam, H. (2007). Th1/Th2 cross-regulation and the discovery of IL-10. J. Exp. Med. *204*, 237. https://doi.org/10.1084/jem.2042fta.
47. Redford, P.S., Boonstra, A., Read, S., Pitt, J., Graham, C., Stavropoulos, E., Bancroft, G.J., and O'Garra, A. (2010). Enhanced protection to Mycobacterium tuberculosis infection in IL-10-deficient mice is accompanied by early and enhanced Th1 responses in the lung. Eur. J. Immunol. *40*, 2200–2210. https://doi.org/10.1002/eji.201040433.
48. Hussain, R., Shiratsuchi, H., Phillips, M., Ellner, J., and Wallis, R.S. (2001). Opsonizing antibodies (IgG1) up-regulate monocyte proinflammatory cytokines tumour necrosis factor-alpha (TNF-alpha) and IL-6 but not anti-inflammatory cytokine IL-10 in mycobacterial antigen-stimulated monocytes-implications for pathogenesis. Clin. Exp. Immunol. *123*, 210–218. https://doi.org/10.1046/j.1365-2249.2001.01439.x.
49. Iyer, S.S., and Cheng, G. (2012). Role of interleukin 10 transcriptional regulation in inflammation and autoimmune disease. Crit. Rev. Immunol. *32*, 23–63. https://doi.org/10.1615/critrevimmunol.v32.i1.30.
50. Ross, S.H., and Cantrell, D.A. (2018). Signaling and Function of Interleukin-2 in T Lymphocytes. Annu. Rev. Immunol. *36*, 411–433. https://doi.org/10.1146/annurev-immunol-042617-053352.
51. Liu, X., Li, F., Niu, H.X., Ma, L., Chen, J.Z., Zhang, Y., Peng, L., Gan, C., Ma, X.M., and Zhu, B.D. (2019). IL-2 Restores T-Cell Dysfunction Induced by Persistent Antigen Stimulation. Front. Immunol. *10*, 2350. https://doi.org/10.3389/fimmu.2019.02350.
52. Niederlova, V., Tsyklauri, O., Kovar, M., and Stepanek, O. (2023). IL-2-driven CD8+T cell phenotypes: implications for immunotherapy. Trends Immunol. *44*, 890–901. https://doi.org/10.1016/j.it.2023.09.003.
53. Meng, L., Tong, J., Wang, H., Tao, C., Wang, Q., Niu, C., Zhang, X., and Gao, Q. (2017). PPE38 Protein of Mycobacterium tuberculosis Inhibits Macrophage MHC Class I Expression and Dampens CD8+ T Cell Responses. Front. Cell Infect. Microbiol. *7*, 68. https://doi.org/10.3389/fcimb.2017.00068.
54. Lewinsohn, D.A., Swarbrick, G.M., Park, B., Cansler, M.E., Null, M.D., Toren, K.G., Baseke, J., Zalwango, S., Mayanja-Kizza, H., Malone, L.L., et al. (2017). Comprehensive definition of human immunodominant CD8 antigens in tuberculosis. NPJ Vaccines *2*, 8. https://doi.org/10.1038/s41541-017-0008-6.
55. Mo, F., Yu, Z., Li, P., Oh, J., Spolski, R., Zhao, L., Glassman, C.R., Yamamoto, T.N., Chen, Y., Golebiowski, F.M., et al. (2021). An engineered IL-2 partial agonist promotes CD8+ T cell stemness. Nature *597*, 544–548. https://doi.org/10.1038/s41586-021-03861-0.
56. Jiang, N., He, J., Weinstein, J.A., Penland, L., Sasaki, S., He, X.S., Dekker, C.L., Zheng, N.Y., Huang, M., Sullivan, M., et al. (2013). Lineage structure of the human antibody repertoire in response to influenza vaccination. Sci. Transl. Med. *5*, 171ra19. https://doi.org/10.1126/scitranslmed.3004794.
57. Hou, D., Ying, T., Wang, L., Chen, C., Lu, S., Wang, Q., Seeley, E., Xu, J., Xi, X., Li, T., et al. (2016). Immune Repertoire Diversity Correlated with Mortality in Avian Influenza A (H7N9) Virus Infected Patients. Sci. Rep. *6*, 33843. https://doi.org/10.1038/srep33843.
58. Achkar, J.M., and Casadevall, A. (2013). Antibody-mediated immunity against tuberculosis: implications for vaccine development. Cell Host Microbe *13*, 250–262. https://doi.org/10.1016/j.chom.2013.02.009.
59. Zeng, L., Ma, X., Qu, M., Tang, M., Li, H., Lei, C., Ji, J., and Li, H. (2024). Immunogenicity and protective efficacy of Ag85A and truncation of PstS1 fusion protein vaccines against tuberculosis. Heliyon *10*, e27034. https://doi.org/10.1016/j.heliyon.2024.e27034.
60. Zeng, L., and Li, H. (2024). Protocol for rapid evaluation of antibody-mediated protection in macrophages using immunofluorescence techniques. STAR Protoc. *5*, 103324. https://doi.org/10.1016/j.xpro.2024.103324.
61. Shugay, M., Bagaev, D.V., Turchaninova, M.A., Bolotin, D.A., Britanova, O.V., Putintseva, E.V., Pogorelyy, M.V., Nazarov, V.I., Zvyagin, I.V., Kirgizova, V.I., et al. (2015). VDJtools: Unifying Post-analysis of T Cell Receptor Repertoires. PLoS Comput. Biol. *11*, e1004503. https://doi.org/10.1371/journal.pcbi.1004503.

62. Ye, T., Jiao, Z., Li, X., He, Z., Li, Y., Yang, F., Zhao, X., Wang, Y., Huang, W., Qin, M., et al. (2023). Inhaled SARS-CoV-2 vaccine for single-dose dry powder aerosol immunization. Nature *624*, 630–638. https://doi.org/10.1038/s41586-023-06809-8.

63. Jia, Q., Wu, W., Wang, Y., Alexander, P.B., Sun, C., Gong, Z., Cheng, J.N., Sun, H., Guan, Y., Xia, X., et al. (2018). Local mutational diversity drives intratumoral immune heterogeneity in non-small cell lung cancer. Nat. Commun. *9*, 5361. https://doi.org/10.1038/s41467-018-07767-w.

64. Ruggiero, E., Nicolay, J.P., Fronza, R., Arens, A., Paruzynski, A., Nowrouzi, A., Ürenden, G., Lulay, C., Schneider, S., Goerdt, S., et al. (2015). High-resolution analysis of the human T-cell receptor repertoire. Nat. Commun. *6*, 8081. https://doi.org/10.1038/ncomms9081.

65. Reuben, A., Gittelman, R., Gao, J., Zhang, J., Yusko, E.C., Wu, C.J., Emerson, R., Zhang, J., Tipton, C., Li, J., et al. (2017). TCR Repertoire Intratumor Heterogeneity in Localized Lung Adenocarcinomas: An Association with Predicted Neoantigen Heterogeneity and Postsurgical Recurrence. Cancer Discov. *7*, 1088–1097. https://doi.org/10.1158/2159-8290.CD-17-0256.

66. Johnson, D.B., Frampton, G.M., Rioth, M.J., Yusko, E., Xu, Y., Guo, X., Ennis, R.C., Fabrizio, D., Chalmers, Z.R., Greenbowe, J., et al. (2016). Targeted Next Generation Sequencing Identifies Markers of Response to PD-1 Blockade. Cancer Immunol. Res. *4*, 959–967. https://doi.org/10.1158/2326-6066.CIR-16-0143.

67. Tumeh, P.C., Harview, C.L., Yearley, J.H., Shintaku, I.P., Taylor, E.J.M., Robert, L., Chmielowski, B., Spasic, M., Henry, G., Ciobanu, V., et al. (2014). PD-1 blockade induces responses by inhibiting adaptive immune resistance. Nature *515*, 568–571. https://doi.org/10.1038/nature13954.

68. Jirous Drulak, M., Grgic, Z., Pluzaric, V., Sola, M., Opacak-Bernardi, T., Viljetic, B., Glavas, K., Tolusic-Levak, M., Perisa, V., Mihalj, M., et al. (2023). Characterization of the TCRbeta repertoire of peripheral MR1-restricted MAIT cells in psoriasis vulgaris patients. Sci. Rep. *13*, 20990. https://doi.org/10.1038/s41598-023-48321-z.

69. Hong, S.B., Shin, Y.W., Hong, J.B., Lee, S.K., and Han, B. (2022). Exploration of shared features of B cell receptor and T cell receptor repertoires reveals distinct clonotype clusters. Front. Immunol. *13*, 1006136. https://doi.org/10.3389/fimmu.2022.1006136.

STAR★METHODS

KEY RESOURCES TABLE

REAGENT or RESOURCE	SOURCE	IDENTIFIER
Antibodies		
Goat Anti-Mouse IgG H&L (HRP)	Abcam	Cat# ab205719; RRID: AB_2755049
Goat Anti-Mouse IgG1 (HRP)	Abcam	Cat# ab97240; RRID: AB_10695944
Goat Anti-Mouse IgG2c heavy chain (HRP)	Abcam	Cat# ab97255; RRID: AB_10680258
Goat Anti-Mouse IgG3 heavy chain (HRP)	Abcam	Cat# ab97260; RRID: AB_10680425
Goat Anti-Mouse IgM mu chain (HRP)	Abcam	Cat# ab97230; RRID: AB_10688258
Goat Anti-Mouse IgA alpha chain (HRP)	Abcam	Cat# ab97235; RRID: AB_10681186
PE anti-mouse CD3	Biolegend	Cat# 100205; RRID: AB_312662
FITC anti-mouse CD4	Biolegend	Cat# 100405; RRID: AB_312690
APC anti-mouse CD8α	Biolegend	Cat# 100711; RRID: AB_312750
PerCp-Cyanine5.5 anti-mouse CD8α	Biolegend	Cat# 100733; RRID: AB_2075239
FITC anti-mouse CD11c	Biolegend	Cat# 117306; RRID: AB_313775
APC anti-mouse CD80	Biolegend	Cat# 104713; RRID: AB_313134
PE anti-mouse CD86	Biolegend	Cat# 159203; RRID: AB_2832567
APC-Cyanine7 anti-I-A/I-E	Biolegend	Cat# 107627; RRID: AB_1659252
Bacterial and virus strains		
Bacillus Calmette-Guérin (BCG) Pasteur (1173P2)	Tsinghua University	N/A
Mycobacterium bovis (M.bovis) (C68004)	China Agricultural University	N/A
Biological samples		
Serum samples from mice	This paper	N/A
Chemicals, peptides, and recombinant proteins		
Middlebrook 7H9 Broth	BD	Cat# 271310
Middlebrook 7H10 Broth	BD	Cat# 262710
Tween 80	Amresco	Cat# 0442
OADC	BD	Cat# 211886
DMEM	Gibco	Cat# C11995500BT
FBS	Eallbio	Cat# A16001DC
100×Penicillin/Streptomycin Liquid	Solarbio	Cat# P1400
FITC	Solarbio	Cat# F8070
PBS	Solarbio	Cat# P1020
4% Paraformaldehyde	Solarbio	Cat# P1110
TMB Single-Component Substrate solution	Solarbio	Cat# PR1200
Polymyxin B	HX-R	Cat# P151602-5g
Amphotericin B	HX-R	Cat# P151366-1g
PrimeSTAR® HS DNA Polymerase with GC Buffer	Takara	Cat# R044Q
BCA Protein Assay	Thermo	Cat# 23227
Imject™ Alum Adjuvant	Thermo	Cat# 77161
Zoletil 50	Virbac	N/A
QuantiCyto® Mouse IFN-γ ELISA kit	Neobioscience	Cat# EMC101g.96
QuantiCyto® Mouse TNF-α ELISA kit	Neobioscience	Cat# EMC102a.96
QuantiCyto® Mouse IL-2 ELISA kit	Neobioscience	Cat# EMC002.96
QuantiCyto® Mouse IL-17/IL-17A ELISA kit	Neobioscience	Cat# EMC008.96
QuantiCyto® Mouse IL-10 ELISA kit	Neobioscience	Cat# EMC005.96

(*Continued on next page*)

Continued

REAGENT or RESOURCE	SOURCE	IDENTIFIER
mouse CD11c MicroBeads UltraPure	Miltenyi	Cat# 130-125-835
Deposited data		
PBS-1 TRB	Accession: PRJNA1188796	https://www.ncbi.nlm.nih.gov/bioproject/PRJNA1188796
PBS-2 TRB	Accession: PRJNA1188786	https://www.ncbi.nlm.nih.gov/bioproject/PRJNA1188786
BCG-1 TRB	Accession: PRJNA1188813	https://www.ncbi.nlm.nih.gov/bioproject/PRJNA1188813
BCG-2 TRB	Accession: PRJNA1188818	https://www.ncbi.nlm.nih.gov/bioproject/PRJNA1188818
BCG-3 TRB	Accession: PRJNA1188991	https://www.ncbi.nlm.nih.gov/bioproject/PRJNA1188991
ALA-1 TRB	Accession: PRJNA1188994	https://www.ncbi.nlm.nih.gov/bioproject/PRJNA1188994
ALA-2 TRB	Accession: PRJNA1189065	https://www.ncbi.nlm.nih.gov/bioproject/PRJNA1189065
ALA-3 TRB	Accession: PRJNA1189044	https://www.ncbi.nlm.nih.gov/bioproject/PRJNA1189044
PBS-1 IGK/IGL	Accession: PRJNA1189259	https://www.ncbi.nlm.nih.gov/bioproject/PRJNA1189259
PBS-2 IGK/IGL	Accession: PRJNA1189260	https://www.ncbi.nlm.nih.gov/bioproject/PRJNA1189260
BCG-1 IGK/IGL	Accession: PRJNA1189298	https://www.ncbi.nlm.nih.gov/bioproject/PRJNA1189298
BCG-2 IGK/IGL	Accession: PRJNA1189302	https://www.ncbi.nlm.nih.gov/bioproject/PRJNA1189302
BCG-3 IGK/IGL	Accession: PRJNA1189313	https://www.ncbi.nlm.nih.gov/bioproject/PRJNA1189313
ALA-1 IGK/IGL	Accession: PRJNA1189322	https://www.ncbi.nlm.nih.gov/bioproject/PRJNA1189322
ALA-2 IGK/IGL	Accession: PRJNA1189331	https://www.ncbi.nlm.nih.gov/bioproject/PRJNA1189331
ALA-3 IGK/IGL	Accession: PRJNA1189346	https://www.ncbi.nlm.nih.gov/bioproject/PRJNA1189346
PBS-1 IGH	Accession: PRJNA1189419	https://www.ncbi.nlm.nih.gov/bioproject/PRJNA1189419
PBS-2 IGH	Accession: PRJNA1189456	https://www.ncbi.nlm.nih.gov/bioproject/PRJNA1189456
BCG-1 IGH	Accession: PRJNA1189455	https://www.ncbi.nlm.nih.gov/bioproject/PRJNA1189455
BCG-2 IGH	Accession: PRJNA1189480	https://www.ncbi.nlm.nih.gov/bioproject/PRJNA1189480
BCG-3 IGH	Accession: PRJNA1189479	https://www.ncbi.nlm.nih.gov/bioproject/PRJNA1189479
ALA-1 IGH	Accession: PRJNA1189481	https://www.ncbi.nlm.nih.gov/bioproject/PRJNA1189481
ALA-2 IGH	Accession: PRJNA1189484	https://www.ncbi.nlm.nih.gov/bioproject/PRJNA1189484
ALA-3 IGH	Accession: PRJNA1189493	https://www.ncbi.nlm.nih.gov/bioproject/PRJNA1189493
Experimental models: Cell lines		
Raw264.7	Beijing Institute of Biotechnology	N/A
Experimental models: Organisms/strains		
Female C57BL/6J mice (6–8 weeks old)	Beijing SiPeiFu Biotechnology	N/A
Software and algorithms		
Flowjo	BD	https://www.flowjo.com/
Graphpad Prism 9	GraphPad Software	https://www.graphpad.com/
Expasy ProtParam	Expasy	https://www.expasy.org/resources/protparam
Expasy ProtScale	Expasy	https://www.expasy.org/resources/protscale
Expasy SWISS-MODEL	Expasy	https://www.expasy.org/resources/swiss-model
Other		
14 mm coverslides	Solarbio	Cat# YA0350
Flow cytometer	BD	BD FACSCalibur™
Nikon A1 confocal microscope	Nikon	Nikon A1
VENTANA DP 200 slide scanner	Roche	VENTANA DP 200
FALCON 40 μm cell strainer	BD	Cat# 352340
FALCON 5 mL polystyrene round-bottom tube	BD	Cat# 352054
Adhesion microscope slides	CITOTEST	Cat# 188105
24 well cell culture cluster	Costar	Cat# 3524
96-well Maxisorp plate	Thermo	Cat# 442404

EXPERIMENTAL MODEL AND STUDY PARTICIPANT DETAILS

Ethics statements

All animals and cell experiments involving virulent *M.bovis* (C68004) and BCG-Pasteur (1173P2) were conducted at the Biosafety Level-3 (BSL-3) Laboratory at China Agricultural University. Animal experiments were approved by the Experimental Animal Welfare Ethical Review Consent of China Agricultural University (license No. AW70902202-2-1).

Bacterial culture

The virulent *M.bovis* (C68004) and BCG-Pasteur (1173P2) strains were cultured in sterile 7H9 medium (Difco, USA) with 10% oleic acid-albumin enrichment (OADC) (BD Biosciences, USA) and 0.05% Tween-80 in BSL-3 Laboratory.[59] The bacteria were used in both animal and cell experiments when they reached the logarithmic growth phase ($OD_{600} \approx 1.0$).

Cell lines

Raw264.7 cells[59,60] were cultured in DMEM medium with 10% fetal bovine serum (FBS) and 1% penicillin/streptomycin (P/S). Upon reaching 80% confluence, the cells were counted and plated. Subsequently, $10^5 \sim 10^6$ cells were seeded in each well of a 24-well cell culture plate and cultured in serum-free DMEM medium before the phagocytosis experiment. All cells were cultured at 37°C with 5% CO2 in a humidified atmosphere. The cell line was routinely checked and confirmed to be mycoplasma-free in our laboratory. No other information related to cell authentication was available.

Mice

Female C57BL/6J mice (6–8 weeks old) were obtained from SiPeiFu Biotechnology (Beijing, China). Before the mouse challenge experiments, the mice were kept in specific-pathogen-free (SPF) conditions, with a controlled temperature range of 18°C–23°C and relative humidity of 40∼60%, for 1 week to recover and acclimatize to the environment.

METHOD DETAILS

Preparation of the Ag85A-LpqH

Mycobacterium tuberculosis H37Rv genome was used as the template for *Ag85A* and *LpqH* amplification by PrimeSTAR HS DNA Polymerase with GC Buffer (Takara), and the two genes were connected by overlap extension PCR (SOE PCR) with a $(GGGGS)_3$ linker. Then the *Ag85A-LpqH* DNA segments were purified and ligated into the pET-21a (+) vector, and the pET-21a-AL plasmid was transfected into *E. coli* BL21 (DE3) strain for fusion protein expression. The fusion Ag85A-LpqH proteins were expressed as aggregated inclusion bodies and then were washed and dissolved in a binding buffer containing 8 M urea (pH 7.9) for Ni-agarose resin purification. The eluted fusion proteins in imidazole were gradually dialyzed with 0–6 M urea and finally dialyzed in PBS (pH 7.4). The purified AL protein was identified by Sodium dodecyl sulfate polyacrylamide gel electrophoresis (SDS-PAGE) and Western Blot(WB). The Expasy ProtParam and Expasy ProtScale tools were used to analyze the physical and chemical properties of AL protein. The Swiss-Model was employed to predict the three-dimensional structure of AL. The purified protein endotoxin levels were assessed using the Tachypleus amebocyte lysate (TAL) assay (Chinese Horseshoe Crab Reagent Manufactory, Xiamen, China). The protein concentration was determined by the BCA Protein Assay (Thermo).

Mouse challenge models

Two vaccination mouse models were established for identifying the protective efficacy of Ag85A-LpqH, and one serum transfer mouse model was used for testing antibodies' protection as described before.[21,59] In the Prevention Model, animals were randomly assigned to four groups: PBS group, BCG group, ALA group, and ALP group. The ALA and ALP groups of mice were subcutaneously immunized with 100 μL subunit vaccines including 20 μg fusion protein AL with 1mg Imject Alum Adjuvant (Thermo, USA) or 20 μg AL with 50 μg Poly IC adjuvant separately thrice with 2-week intervals. The BCG and PBS control groups were administered subcutaneously with 5×10^5 colony-forming units (CFU) of BCG Pasteur (1173P2) in 100 μL PBS or 100 μL PBS individually.

For the Prime-Boost Model, mice were randomly divided into four groups: PBS, BCG, ALA, and ALP group. The BCG, ALA, and ALP groups were immunized with 5×10^5 CFU of BCG Pasteur (1173P2) individually. The PBS control group was administered 100 μL PBS. After 4 weeks, all two trial groups were subcutaneously immunized thrice with 100 μL subunit vaccines (ALA or ALP), at 2-week intervals. Two weeks after the final immunization (10 weeks after BCG immunization in the BCG group), The mice were anesthetized with a subcutaneous injection of PBS-diluted Zoletil 50 (50 mg/kg; Virbac, France), and after that, all the mice were challenged with virulent *M.bovis* strain via the intranasal route at 200 CFU for chronic infections. Three mice were sacrificed to determine the initial lung infection dose in 24 h. For the serum transfer model, five groups were involved in this experiment: The control group, PBS group, BCG group, and ALA group each consisting of 5 C57BL/6J mice aged 6–8 weeks. After a week of acclimatization in a barrier environment, each mice received 300 μL of PBS or specific serum obtained from mice immunized with ALA, PBS, or BCG and then infected with 300 CFU *M.bovis* (C68004) 5 h post-immunization. Two weeks after infection, the cervical dislocation method was used to euthanize the mice, and the mice were immersed and sterilized in 75% ethanol for about 5 min before dissection.

In this study, the infected lungs and spleens tissue were harvested and separately placed in sterile grinding tubes with sterile PBS and grinding beads, and were homogenized using a tissue homogenizer (Kangtao Tech, China). Then the homogenates were diluted and plated on 7H10 agar supplemented with 10% OADC, amphotericin B (50 μg/mL), and polymyxin B (50 μg/mL). After a four-week incubation at 37°C, the CFUs on plates were conducted to evaluate the protection efficacies of the vaccine and serum antibodies.

Histopathological analysis

The lung tissues were fixed in 10% formaldehyde for one week and used for paraffin-embedded sectioning and Hematoxylin/eosin (HE) staining. The tissue sections were scanned by VENTANA DP 200 slide scanner (Roche Diagnostics, Switzerland), and the lung pathological damage lesions were quantified by lung pathology evaluation and rating. Lung lesions were categorized into five grades, Grade 0: normal lung tissue without inflammation, edema, or hemorrhage. Grade 1: a minimal amount of inflammatory cell infiltration around the alveoli. Grade 2: a significant area of diffuse inflammatory cell infiltration or hemorrhage surrounding the alveoli. Grade 3: a substantial amount of inflammatory cell infiltration and edema around the alveoli, along with 1∼3 evident necrosis foci or a lower 30% pathological damage area and other pathological features. Grade 4: a notable amount of inflammatory cell infiltration and edema around the alveoli, accompanied by 3∼5 evident necrosis foci or a 30–50% pathological damage area and other pathological characteristics. Grade 5: a considerable amount of inflammatory cell infiltration and edema around the alveoli, accompanied by more than 5 evident necrosis foci or an exceeded 50% pathological damage area and other pathological features.

Enzyme-linked immunosorbent assay (ELISA)

Blood samples were obtained from the mice via the tail vein 2 weeks after each immunization and 4 weeks after infection. In the Prevention group, blood samples were collected 2 weeks following the first, second, and third immunizations, as well as 4 weeks after infection. For the Prime-Boost group, blood samples were taken 2 weeks after each of the three boosted immunizations and 4 weeks post-infection. The collected blood samples were left to sit overnight at 4°C, followed by centrifugation the next day to obtain serum samples which were then frozen at −80°C. *M.bovis* in the logarithmic growth phase was centrifuged, washed with PBS, and heat-inactivated before conducting the ELISA experiment. 1×10^7 CFU heat-inactivated *M. bovis* were suspended in water and plated in each well of a 96-well Maxisorp plate (Thermo, Denmark). Then the plates were dried in an oven at 60°C, followed by the fixation of bacteria with pre-cooled methanol at room temperature for 15 min. 5% skim milk (BD, USA) in PBS was used as a blocking agent at room temperature for 2 h. Serum samples diluted at 1:3000 were added to each well of the ELISA plate (100 μL per well) and incubated at room temperature for 1 h. Subsequently, a 1:20000 dilution of anti-mouse IgG, IgG1, IgG2c, IgG3, IgM, and IgA (Abcam, UK) as secondary antibodies were incubated at room temperature for 1 h. Between each step, plates were washed five times with PBST (PBS with 0.05% Tween 20). Finally, the TMB Single-Component Substrate solution (Solarbio, China) was used for color development and the OD490 of each well was measured by a multifunction microplate reader (Tecan, Switzerland).

Preparation of single-cell suspensions

The mice were euthanized by cervical dislocation and then immersed in 75% ethanol for 5 min before dissection. The Lymph nodes and spleens were aseptically removed, minced, filtered through a sterile 40 μm filter (BD, USA), and centrifuged to collect a single-cell suspension. Additionally, the femur and tibia were isolated to harvest bone marrow cells. The epiphyses of the femur and tibia were cut with ophthalmic scissors. Then the bone marrow cells were flushed out with RPMI1640 serum-free medium (Gibco, USA) and filtered through a sterile 40 μm filter to obtain a single-cell suspension. Splenocytes and Bone marrow cells also need a Red Blood Cell Lysis Buffer (Solarbio, China) to lyse red blood cells and obtain the cells that the experiment needs. These cells were washed, centrifuged, re-suspended, and counted for subsequent experiments.

Cytokines detection assay

The isolated primary cells were plated in a 12-well plate (Corning, USA) with 10^7 cells per well, and stimulated with 10 μg/mL of BCG lysates or AL proteins. After a 12-h co-incubation in a cell culture incubator at 37°C with 5% CO_2, the cells were centrifuged, and the supernatants were frozen at −80°C for cytokine assays. The pellet cells were then prepared for flow cytometry staining. The levels of IFN-γ, TNF-α, IL-2, IL-17, and IL-10 cytokines were detected using ELISA kits (Neobioscience, China) following the manufacturer's instructions to assess the cytokines level in each group after immunization.

Cell analysis by flow cytometry

The harvested pellet cells which were stimulated for 12 h or without stimulation were initially incubated with Fc receptor blocking agent TruStain FcX (BioLegend, USA) at 4°C for 10 min. Subsequently, different types of cells were incubated with various cell surface marker antibodies purchased from BioLegend, such as PE anti-mouse CD3 (Cat#100205; Clone:17A2), FITC anti-mouse CD4 (Cat#100405; Clone: GK1.5), APC anti-mouse CD8α (Cat#100711; Clone: 53–6.7), PerCp-Cyanine5.5 anti-mouse CD8α (Cat#100733; Clone: 53–6.7), FITC anti-mouse CD11c (Cat#117306; Clone: N418), APC anti-mouse CD80 (Cat#104713; Clone:16-10A1), PE anti-mouse CD86 (Cat#159203; Clone: A17199A) and APC-Cyanine7 anti-I-A/I-E (Cat#107627; Clone: M5/114.15.2) fluorescent antibodies at 4°C for 30 min to identify the alterations of cell subtypes. Then the cells were washed, re-suspended in cell staining buffer (BioLegend, USA), and analyzed using a BD FACSCalibur flow cytometer or BD FACSVerse flow cytometer (BD Biosciences, USA) for 2 h.

Mixed lymphocyte reaction assay

The tibia and fibula of the mice were aseptically removed, followed by flushing out the cells with PBS and lysing the red blood cells. The bone marrow cells (BMs) were then cultured in a medium containing 20 ng/mL GM-CSF and 10 ng/mL IL-4. 6 days later, the cells were removed and the mouse CD11c MicroBeads UltraPure (Miltenyi, Germany) was used for obtaining purified BMDCs. Then the BMDCs were stimulated with 10 μg/mL specific antigens for 24 h after plating. The stimulated mature BMDCs were treated with mitomycin C and then incubated with spleen lymphocytes for 72 h to detect lymphocyte differentiation.

Macrophage phagocytosis assay

For the phagocytosis experiment, Raw264.7 cells were infected with FITC-labeled log phase BCG (MOI of 5:1) for 2 h. Mice serum samples were added at the final concentration of 10% medium (v/v). After infection, Raw264.7 cells were washed, fixed with 4% paraformaldehyde for 2 h, and analyzed using a BD FACSCalibur flow cytometer (BD Biosciences, USA) to count the ratio of phagocytosed bacterial cells. For the counting macrophage phagocytosis experiment, Raw264.7 cells were infected with log phase BCG (MOI of 5:1) in 10% mice serum of DMEM medium for 2 h. Then the Raw264.7 cells in plates were washed, lysed using 0.1% Triton X-100, diluted, and plated on 7H10 plates. After 3–4 weeks of incubation at 37°C, the colony-forming units (CFUs) were counted and recorded to measure the phagocytosis efficiency.

BCR and TCR repertoires sequencing and analysis

The mice immunized with PBS, BCG, and ALA in the prevention model were chosen to perform the B cell receptor (BCR) and T cell receptor (TCR) deep sequencing. Following immunization, mice were sacrificed, and the splenocytes were extracted. RNA extraction was performed using the RNeasy Plus Mini Kit (Qiagen, Germany) following the manufacturer's protocol. The extracted RNA samples underwent next-generation sequencing (NGS) for profiling BCR and TCR repertoires using the ImmuHub TCR profiling system (ImmuQuad Biotech, Hangzhou, China). Briefly, a 5′ rapid amplification of cDNA ends (RACE) unbiased amplification was carried out, incorporating unique molecular identifiers (UMIs) to control bottlenecks, correct PCR and sequencing errors, and remove duplicates. Sequencing was performed on an Illumina NovaSeq system with PE150 mode. Nucleotide and amino acid sequences of CDR3 of TRB, IGH, and IGL were determined. VDJtools was employed for further analysis of the TCR/BCR clonotype data.[61,62] Various related indices were analyzed such as Shannon's index, Clonality, DE50 index, Singleton index, and so on. (INDEX: Shannon's entropy index: H' = -$\sum$pi(ln pi)[63,64]; Clonality = 1-diversity/ln productive uniques[65–67]; DE50 = nb rearrangements accounting for 50% total map intensity/total nb rearrangements present[68,69]; Singleton = Single clone counts/Total clone counts). The BCR IGH, IGL, and TCR TRB analyses algorithm and plotting were performed with R (version 3.5.1).

QUANTIFICATION AND STATISTICAL ANALYSIS

Statistical analysis was performed using GraphPad Prism 9 software, and data were expressed as absolute numbers or mean ± standard deviation (mean ± SD). Flow cytometry data were analyzed using FlowJo software. Experimental data were analyzed using one-way analysis of variance (ANOVA) and Tukey's multiple comparison test (ns: not significant; *$p < 0.05$; **$p < 0.01$; ***$p < 0.001$; ****$p < 0.0001$).